HEFAT2014
10th International Conference on Heat Transfer, Fluid Mechanics and Thermodynamics
14 – 16 July 2014
Orlando, Florida

DISTRIBUTED HEAT CONVERSION TECHNOLOGIES BASED ON ORGANIC-FLUID CYCLES FOR A HIGH-EFFICIENCY AND SUSTAINABLE ENERGY FUTURE

Markides C.N.*
*Author for correspondence
Clean Energy Processes Laboratory,
Department of Chemical Engineering,
Imperial College London,
London SW7 2AZ,
United Kingdom,
E-mail: c.markides@imperial.ac.uk

ABSTRACT

This paper presents and discusses the emergence of two distinct classes of energy conversion systems based on thermodynamic vapour-phase heat engine cycles undergone by organic working fluids, namely organic Rankine cycles (ORCs) and two-phase thermofluidic oscillators (TFOs). Each type of system has its own distinctive characteristics, advantages and limitations. ORCs are a more well-established and mature technology, are more efficient, especially with higher temperature heat sources and at larger scales, whereas TFOs have the potential to be more cost-competitive, in particular at lower temperatures and at smaller scales. Specifically, ORC systems are particularly well-suited to the conversion of low- to medium-grade heat (i.e. hot temperatures up to about 300 – 400 °C) to mechanical or electrical work, and at an output power scale from a few kW up to 10s of MW. Thermal efficiencies in excess of 25% are achievable at the higher temperatures, and efforts are currently in progress to develop improved ORC systems by focussing on advanced architectures, working fluid selection, heat exchangers and expansion machines. Correspondingly, TFO systems are a more recent development aimed at the affordable conversion of low-grade heat (i.e. hot temperatures from 20 – 30 °C above ambient, up to about 100 – 200 °C) to hydraulic work for fluid pumping and/or pressurisation. Ultimately, TFOs could emerge at scales of up to a few hundred W and with a thermal efficiency of the order of a few % points. The two energy conversion systems are complementary, and together have a great potential to be used for distributed power generation and improved energy efficiency, leading to primary energy (i.e. fuel) use and emission minimisation. Relevant applications and fields of use include the recovery of waste heat and conversion to useful work including mechanical, hydraulic or electrical energy, or the effective utilisation of renewable energy sources such as geothermal, biomass/biogas and solar energy.

INTRODUCTION AND MOTIVATION

Overview and Problem Statement

The recent heightened involvement in the energy debate, in the scientific community, government and policy circles, and the public domain, has given rise to an intensified interest and rapid developments in a variety of fuel-to-power and heat-to-power conversion technologies. These technological developments have come from all of the areas of energy supply, conversion, storage and provision, spanning a range of scales and diverse applications. In particular, two important aspects of the energy challenge concern: (i) the improved utilisation of the vast amount of rejected energy to the environment, in particular in the form of waste heat from domestic and commercial settings and from a wide range of industrial processes, as well as (ii) the harnessing of renewable and sustainable energy sources, such as the solar resource, for the provision of heat and power, and also, depending on the application, cooling [1].

In the following paragraphs, we will attempt to justify rationally the interest in such technologies by considering both performance and cost, to discuss aspects of scale and the use of distributed and centralised energy systems, and to identify a number of suitable systems that can contribute in the medium term towards a high-efficiency and sustainable energy future. The conversion technologies of interest here are aimed at the domestic (1 – 10 kWe) and commercial/industrial (10 – 100s of kW) sectors, thus covering a range of power output scales from 1 kW to 1 MW. In addition, we focus on heat source temperatures from 20 – 30 °C above ambient to 400 °C.

Global Energy Outlook

Wasted energy in the form of rejected heat to the environment in both the US and the EU-27 accounts for approximately 60% of all consumed net primary energy, and has remained relatively constant around this value over the past

decade. In the US ~ 60 EJ (1 EJ ≡ 1×10^{18} J) of energy are lost in the form of waste heat per ~ 40 EJ of useful energy consumed per year [2], while the EU-27 figures are ~ 45 EJ and ~ 30 EJ per year, respectively [3]. The total, worldwide amount of rejected heat is estimated as being close to ~ 250 EJ, or 55% of the total energy flow of ~ 490 EJ per year [4].

Interestingly, losses from electrical power generation and transportation jointly amount to between 70 – 80% of the total wasted energy; being closer to 70% in the EU, ~ 73% globally and closer to 80% in the US. Of these two sectors, the relative contribution of electrical power generation towards this wasted energy is greater than that of transportation by a factor of between 1.2 – 2.0 (US: ~ 1.2, EU: ~ 1.6, World: ~ 1.9). Further, the overall energy conversion efficiencies, i.e. useful output energy per unit primary energy supply, is about 30 – 40% for electrical power generation (US: ~ 32%, World: ~ 37%, and EU: ~ 42%), and 20 – 25% for transportation (US and EU: ~ 20%, World: ~ 26%). It is noted that the EU value of 42% includes heat recovery and use for heating in combined heat and power schemes. If this is excluded, the electrical power only per unit energy input associated with power generation in the EU drops to ~ 35%, in line with the US and World values.

Based on the analysis above, it is possible to conclude that: (i) exploiting the vast amount of wasted energy in the form of rejected heat to the environment in two key sectors, namely electrical power generation and transportation, has the by far the greatest potential to reduce global demand for primary energy, as well as all harmful emissions and other risks associated with the provision and conversion of this energy; and (ii) electrical power generation has a greater relative contribution to the energy losses compared to transportation, but both remain sizeable contributions, especially when considering that power generation is generally more 'efficient' than transportation, in which case the potential to enhance efficiency becomes slightly better for the latter.

Now, electrical power generation and transportation are dominated currently by the practice of fossil fuel (coal, liquid fuels, gas) combustion in order to produce high-grade (i.e. high-temperature) thermal energy, and the subsequent use of thermodynamic heat engine systems to transform this energy to mechanical work (motion or electricity). Only a limited number of different types of heat engine are presently employed for (the majority of) this purpose: (i) external combustion engines: gas (Joule/Brayton) and steam (Rankine) cycles, and (ii) internal combustion engines, Diesel and Otto cycles.

Efficiency Considerations

Figure 1 is a performance map that shows the thermal efficiencies, η_{th}, of various heat engines over a range of heat source temperatures, T_{hot}, from 100 °C to 1400 °C. Also shown in this figure is the relative performance of thermoelectric generators (TEGs), a competing technology for thermal energy conversion directly to electricity based on the Seebeck effect.

The circular points in Figure 1 represent systems based on ORC and Kalina (ammonia-water) cycles in actual waste heat and geothermal applications up to $T_{hot} \approx 350$ °C [5]. The square point represent, in order of increasing heat source temperature:

- $T_{hot} \approx 300 – 400$ °C: large-scale nuclear-powered steam/Rankine cycles;
- $T_{hot} \approx 400 – 600$ °C: large-scale concentrated solar power (CSP) Rankine cycles; and,
- $T_{hot} \approx 550 – 800$ °C: large-scale conventional coal-fired Rankine cycles and advanced supercritical coal Rankine cycles.

In addition, the diamond points in the same figure are taken from Refs. [5,6] and represent the performance of Stirling engine cycles, while the triangle at $T_{hot} \approx 700$ °C represents a highly concentrated solar dish Stirling cycle. The stars are from the (travelling-wave) thermoacoustic (TA) engine system reported in Ref. [7]. Internal combustion engines (ICEs), based on both Diesel and Otto cycles, are also shown on the far left-hand side of the figure, along with a combined-cycle gas turbine (CCGT), i.e. Joule/Brayton top cycle plus Rankine bottoming cycle, at $T_{hot} > 1300$ °C.

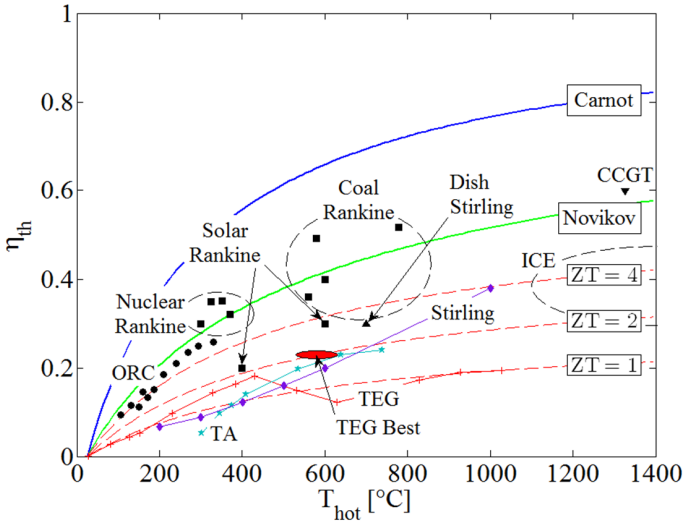

Figure 1 Thermal efficiency, η_{th}, of thermodynamic heat engines and TEGs over a range of heat source temperatures, T_{hot}. The circles represent actual ORC and Kalina cycles in waste heat and geothermal applications; the squares are for various Rankine cycles; the triangles for solar dish Stirling and CCGT cycles; the diamonds for conventional Stirling; and the stars for TA engines. The solid red line is the current performance of TEGs, with the three dashed red lines indicating TEG figure-of-merits $ZT = 1$, 2 and 4.

The maximum thermodynamic limit imposed by the Carnot efficiency, $\eta_C = \eta_{th} = 1 - T_{cold}/T_{hot}$, is indicated in Figure 1 by the blue line, and the Novikov and Curzon-Ahlborn efficiencies result from endoreversible analyses, $\eta_{th} = 1 - (T_{cold}/T_{hot})^{0.5}$, is indicated by the green line. In both cases a heat sink is selected with a fixed temperature $T_{cold} = 25$ °C.

Furthermore, the solid red line indicates current performance of TEGs, and the three dashed red lines indicate theoretical efficiencies, $\eta_{th} = \eta_C \times [(1 + ZT)^{0.5} - 1]/[(1 + ZT)^{0.5} + T_{cold}/T_{hot}]$, attained by TEGs given figure-of-merits: $ZT = 1$, 2 and 4. As above, a heat sink temperature of $T_{cold} = 25$ °C is used. In this expression the modifying ratio multiplied by the Carnot efficiency accounts for Joule losses (i.e. losses due to parasitic electrical power dissipation and conversion to heat)

and other inherent irreversible processes in TEGs [8]. In evaluating the performance of actual TEG systems $ZT(T_{hot})$ values for different materials were taken [9,10] and used in this expression at the corresponding heat source temperature, T_{hot}, at which they are mentioned in the stated references. The dashed lines where generated with this same expression, assuming that the value ZT is maintained constant over the range of investigated heat source temperatures, T_{hot}. It is noted that current 'best' performance in terms of ZT (also indicated in Figure 1), attained under laboratory conditions, is around 2.1 at 800 K/530 °C [11] and 2.2 at 900 K/630 °C [12], while commercially available systems can be found with ZT values of unity ($ZT \approx 1$). Ref. [13] also mentions a material with a ZT value of 3.5, but this does not yet lend itself to being produced in bulk quantities as would be required in practical applications.

The value of $ZT = 4$ is referred to in Ref. [13] as being 'ambitious', yet possibly feasible. The opinion of the present author is that a significant breakthrough will be required to attain a working, commercially available and economically competitive TEG system operating at an average value of $ZT = 4$, and even then it is unlikely to emerge in the range of temperatures that are of interest here, i.e. < 400 °C. Therefore, the inescapable conclusion from Figure 1, which is reached also by the author of Ref. [13], is that although TEGs may yet become appropriate for small-scale applications which require power outputs < 100 W, it is unlikely that they will play a role in the type and range of applications that are considered in the present work, i.e. > 1 kW and 20 – 400 °C.

Moreover, Figure 1 suggests that ORCs are the preferred heat conversion technology at temperatures lower the 400 °C. It is both interesting and important to consider the reason for which ORCs have the potential to outperform other systems, including conventional Rankine cycles at these lower temperatures, especially in the power range of our focus applications, i.e. 1 kW – 1 MW. We proceed do to this below.

Figure 2 shows a contour plot of the normalised power output from an infinite series of infinitesimal ideal (Carnot cycle) engines operating between (varying) heat source *and* heat sink temperatures. We consider a heat source fluid stream entering a 'hot' heat exchanger (HHX) within which an infinitesimal amount of heat, $d\dot{Q}_{hot}$ (> 0) is transferred from the fluid stream to the working fluid in each successive cycle. During this process the enthalpy of the hot fluid stream decreases according to $d\dot{H}_{hot} = -d\dot{Q}_{hot}$. Similarly, a heat sink fluid stream enters a 'cold' heat exchanger (CHX) within which heat is rejected from the cycles to the fluid stream. The heat source stream enters the HHX at a temperature $T_{hot,in}$, and experiences a total temperature drop through that heat exchanger ΔT_{hot}, such that $\Delta\dot{H}_{hot} = (\dot{m}c_p)_{hot}\Delta T_{hot}$, while the heat sink stream enters the CHX at a temperature $T_{cold,in}$, and experiences a temperature rise ΔT_{cold}, such that $\Delta\dot{H}_{cold} = (\dot{m}c_p)_{cold}\Delta T_{cold}$. For simplicity, but without loss of generality, we consider the case when the two streams have equal duties, $\dot{m}c_p$. Assuming that the heat exchangers are ideal, with no losses to the surroundings, the enthalpy flow difference across the HHX is also equal to the total heat transferred to the working fluid in all of the cycles, $\Delta\dot{H}_{hot} = -\dot{Q}_{hot}$. Note that this analysis is subtly different from a maximum work (exergy) analysis, in which heat is rejected from a similar arrangement to a *constant* 'dead' state temperature, rather than to a varying cooling stream temperature as is done here.

The horizontal axis in Figure 2 is the inlet temperature of the heat source fluid stream to the HHX, $T_{hot,in}$, while the vertical axis is the temperature drop of the same stream through the HHX normalised by the inlet temperature, $\Delta T_{hot}/T_{hot,in}$. The inlet temperature of the heat sink fluid stream to the CHX is set to $T_{cold,in} = 20$ °C. Also superimposed on this plot are two lines. The white line is a locus of the maximum power output at each value of $T_{hot,in}$, which corresponds to a monotonically increasing value of $\Delta T_{hot}/T_{hot,in}$. The red line traces the output of this ideal arrangement for a given application with a fixed heat flow, $\dot{Q}_{hot}$, and a fixed duty, $\dot{m}c_p$. This case has a fixed heat flow per unit duty, $\dot{Q}_{hot}/(\dot{m}c_p)$, chosen here arbitrarily to be equal to 100.

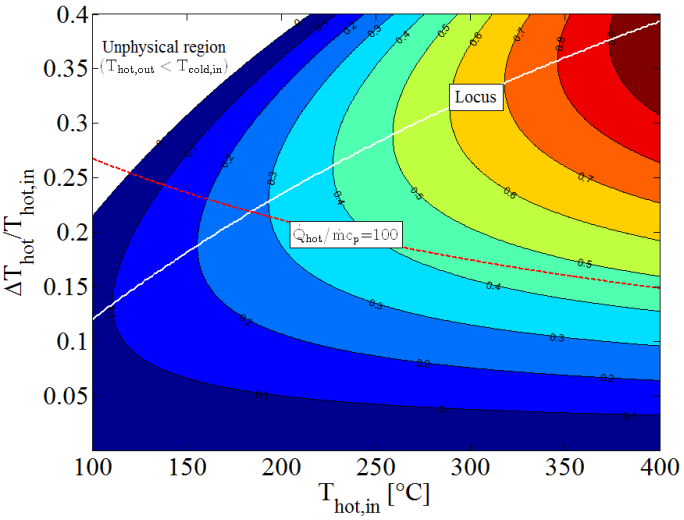

Figure 2 Effect of heat source cooling and heat sink heating on ideal (maximum) cycle power output per unit heat duty $(\dot{m}c_p)_{hot} = (\dot{m}c_p)_{cold}$, showing locus of maximum net output power, with $T_{cold,in} = 20$ °C.

Two important interpretations emerge from Figure 2. Firstly, the *ideal* conversion of heat at higher temperatures such that maximum power is extracted requires that the normalised heat source temperature drop is high. For instance, consider an ideal system to be used for converting heat at $T_{hot,in} = 100$ °C. For this system, maximum power is attained for a normalised heat source temperature drop of $\Delta T_{hot}/T_{hot,in} = 0.12$. This corresponds to a temperature drop of $\Delta T_{hot} = 45$ °C, from 100 °C to 55 °C through the HHX. At the same time (not shown in the figure) the cold temperature through the CHX increases from 20 °C to 60 °C. Conversely, consider a second system to be used for converting heat at $T_{hot,in} = 400$ °C. Maximum power for this second system is attained for a normalised heat source temperature drop of $\Delta T_{hot}/T_{hot,in} = 0.4$, which corresponds to a temperature drop of $\Delta T_{hot} = 270$ °C, from 400 °C to 130 °C. The cold temperature though the CHX increases from 20 °C to 215 °C.

Now, for a given duty of the heat source and heat sink fluid streams the second system will be ~ 6 times larger in terms of the heat input to the cycle and, thanks to its higher efficiency, more than 10 times larger in terms of the power output. In other words,

for the same heat source fluid-stream duty, higher temperature heat sources and thermodynamic heat engine systems that are more appropriate for utilising these higher heat source temperatures more effectively are better suited to large-scale (centralised) power generation, whereas lower temperature sources and systems that are capable of converting these effectively are more suited to smaller-scale (distributed) power generation. The increased stream duty expected in the larger systems will only act to amplify this distinction.

Secondly, an important difference between the employment of water and organic compounds as working fluids (i.e. between conventional Rankine cycles and ORCs) is the much greater specific enthalpy associated with heat addition of the former. An increased specific enthalpy associated with heat addition will also lead to an increased heat (per unit mass of working fluid) intake into the cycle shifting the ideal operation of this cycle towards higher temperatures and larger systems as a consequence of the discussion in the previous paragraphs. It is also true that the *specific* power output from Rankine cycles, even at low temperatures, can be higher than ORC equivalents. However, this advantage is overcome and negated by the need to use much lower working fluid mass flow-rates in Rankine cycles operating at low temperatures compared to ORCs, owing to the large differences in specific enthalpy of heat addition.

Cost Considerations

An acceptable performance from a technical standpoint can be judged based on indicators such as primary energy/fuel efficiency, emissions, flexibility of operation and ability to match variable demand, etc. Yet, beyond these purely technical considerations, the widespread deployment of any successful solution to the energy challenge must be associated with, either a cost benefit or at the very least a cost level that is affordable and economically justifiable to the end-user or investor [1].

In conventional power generation, fuel costs are the single largest contributor towards the total cost of electricity. Consider, for example, a typical coal-fired steam power plant with a typical efficiency of 38 – 40%, a capital cost in the region of 820 – 860 £/kW, an additional operating and maintenance cost of 20 – 30 £/kW, and an economic life expectancy of 30 years [14]. This plant has a total levelised electricity cost (LEC) of 33 £/MWh produced over the lifetime of the plant. Moreover, the largest single contributor towards this cost is the cost of fuel, which amounts to 35%. The case is even stronger for gas-fired power plants. A typical simple open-cycle gas turbine (OCGT) power plant with a typical efficiency of 39 – 43%, a capital cost of 330 £/kW, an operating and maintenance cost of 35 £/kW and an economic life expectancy of 20 years has a total LEC of 35 £/MWh of which more than 60% is attributed to the fuel. Similarly, closed-cycle combined gas turbine (CCGT) power plant with a typical efficiency of 58 – 60%, a capital cost of 300 £/kW, an operating and maintenance cost of 25 £/kW and an economic life expectancy of 25 years has a total LEC of 35 £/MWh of which 60% is again attributed to the purchase of gas [14].

Hence, beyond its formal definition, it is reasonable to argue that, for the case of conventional power generation, the thermal efficiency is also a figure-of-merit that is a reasonable measure of the electrical energy output (and thus profit) *per unit total cost*. This cannot be said for systems whose energy input is not associated with a significant cost, such as waste heat conversion technologies. In this case, the total cost is dominated by the up-front initial investment required for the necessary capital expenditure, and consequently the figure-of-merit that is the electrical energy output (i.e. profit) per unit total cost must be evaluated directly as the electrical energy output per unit installation cost, or at least per unit capital cost. In both cases, this figure-of-merit goes some way towards reflecting the true economic viability of such systems, in a way that thermal efficiency alone cannot.

Distributed Energy Conversion Systems

In the previous section a brief overview was presented of the rationale that is acting to motivate a particular interest in technologies that are capable of converting wasted heat to additional useful work (either mechanical, hydraulic or electrical). In particular, it was argued that it is beneficial to consider cost-effective technologies that can be used for waste heat recovery and conversion in: (i) more efficient power generation (possibly in co-generation, or tri-generation mode, where the final rejected heat is also harnessed for heating and/or cooling), and (ii) transport applications. Additionally, technologies are sought which are diverse enough to be suitable for the conversion of renewable sources of energy such as geothermal heat, biomass/biogas and solar energy.

A series of technologies are being proposed that aim to respond to the stated requirements, in particular for distributed power generation and simultaneous heat provision. Benefits from an increased deployment of distributed power generation solutions include enhanced reliability and security, reduced losses from energy transmission and distribution, as well as reduced infrastructure and maintenance costs for transmission and distribution, and easier plant sizing [15,16].

It is implied that distributed systems will be smaller in scale than centralised equivalents and will not benefit from the economies of scale the latter enjoy. In addition, one must remain aware of the fact that centralised, larger-scale systems will retain an edge in plant efficiency, but that this efficiency will be compromised by increased transmission/distribution losses from the plant to the consumer/end-user. In many cases these losses are not negligible, and typically amount to a reduction of the plant's efficiency by 5 – 10% points.

Organic-Fluid Cycles

The use of organic working fluids offers certain advantages over conventional vapour-cycle heat engines (e.g. Rankine) and gas-cycle engines (e.g. TA and Stirling), which arise from the properties of the available fluids (and mixtures thereof). These include a reduced reliance on superheating to avoid problematic condensation in the case where turbines are used for expansion and work extraction, simpler and more affordable evaporator and condenser designs owing to the more flexible selection of the thermodynamic conditions, including pressure, high heat transfer rates and a greater degree of freedom in designing the single and two-phase processes in key components. These factors are examined in the following sections.

ORGANIC RANKINE CYCLES

Technology Outline

ORC systems have been indicated in the previous sections as a highly appropriate technology for the conversion of heat at temperatures lower than 400 °C. ORC systems with suitable working fluids can be used at higher temperatures, but we will focus on this temperature range in the present paper. ORCs are a relatively mature technology, with operational experience available since the 1960s. Currently, more than 600 ORC plants are in operation worldwide, with a cumulative capacity in excess of 2000 MW. A typical layout of a simple sub-critical, non-regenerative ORC system is shown in Figure 3, together with a cycle on a *T*–*S* diagram with R-245fa as the working fluid. The main components of the system are a feedpump (this can be multistage), evaporator (this can comprise a number of heat exchanging components, including a superheater), expander/turbine (again this can comprise a number of stages) and condenser (including a de-superheater). A regenerator can also be used to recover some of the heat rejected downstream of the expander (Point 4 in the diagram) and to use this to perform part of the heating downstream of the pump (Point 2).

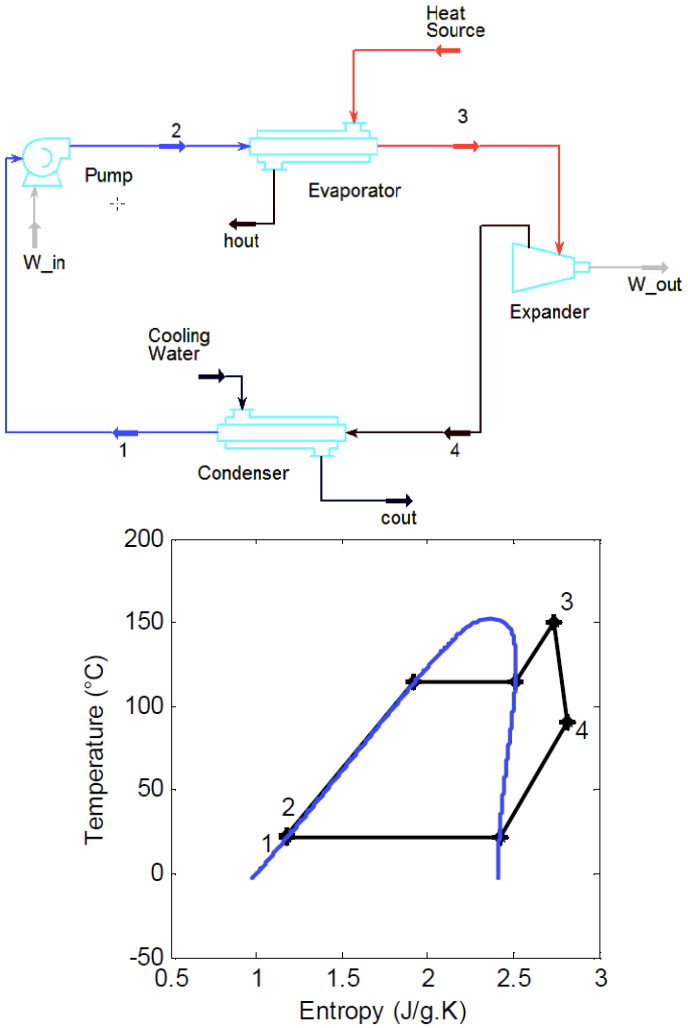

Figure 3 Sub-critical non-regenerative ORC system and cycle on a *T*–*S* diagram with R-245fa as the working fluid.

ORCs are associated with a number of advantageous features compared to water-steam Rankine cycles. Firstly, unlike wet fluids such as water, dry or isentropic organic fluids (see Figure 4) have positively sloped or vertical dry saturation curves. Therefore, they do not require a significant degree of superheating in order to avoid condensation and droplet formation in turbines/expanders. Such a scenario can cause mechanical damage to the turbine blades, and also degrade the thermodynamic performance of this component. The former would not apply to more structurally robust expander designs (e.g. reciprocating piston expanders), but the latter would remain.

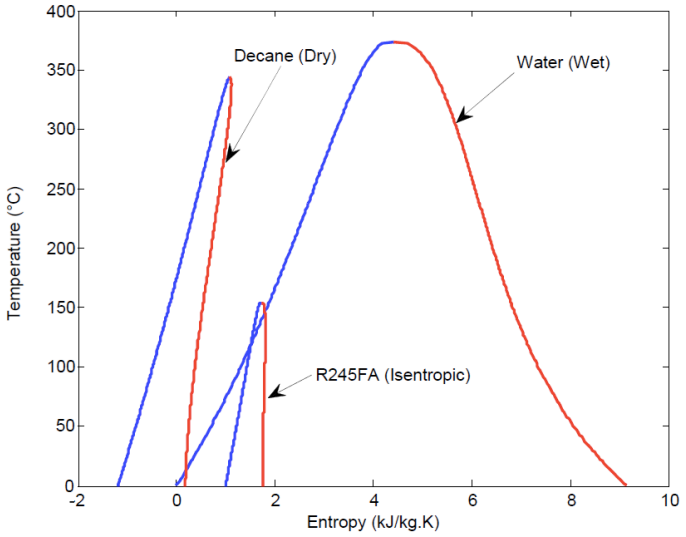

Figure 4 Saturation (phase equilibrium) curves for dry, wet and isentropic fluids on a on a *T*–*S* diagram.

In the case of wet working fluids, the desire to keep the flow through the expander entirely outside of the saturation region, and hence for the exit state from the expander to also be outside the saturation region, translates to a requirement for significant superheating prior to entry into the turbine. This is illustrated in Figure 5, where the absence of adequate superheating leads to an intersection of the dry saturation curve, and thus, expansion into the saturation (two-phase) region.

Secondly, it is advantageous thermodynamically to expand the working fluid to the lowest possible pressure that corresponds to condensation and heat rejection at a temperature as close as possible to the cooling stream temperature. Assuming this is at ambient conditions (20 – 25 °C), the condensation temperature would be a few degrees higher than this, as determined by the pinch temperature difference in the condenser. For water, a saturation temperature of 30 °C corresponds to an absolute saturation pressure close to 0.04 bar. The large pressure difference between the surrounding atmosphere and any components that operate at such low pressures can give rise to the ingress of air into the cycle with significant detrimental effects on system performance. The design of components that can operate reliably at such a degree of sub-atmospheric pressures is difficult and expensive. Conversely for R-245fa the saturated condensation pressure at a saturated temperature of 30 °C is 1.8 bar, which is above atmospheric.

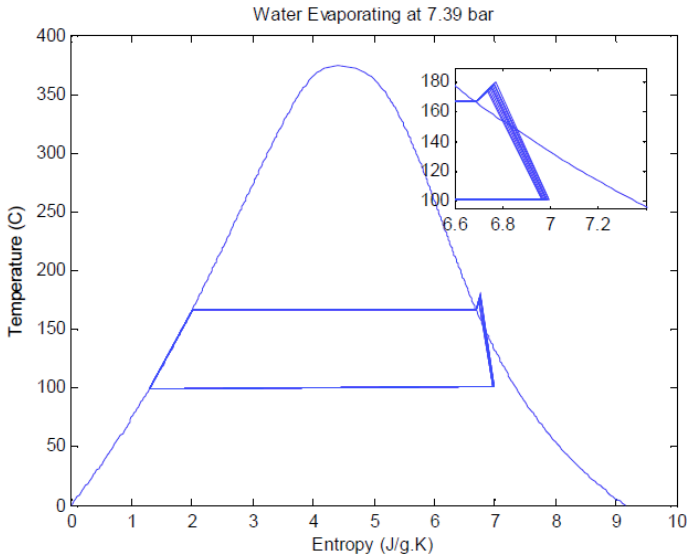

Figure 5 Low-temperature water-steam Rankine cycle, showing expansion into the saturation region; compare this with the ORC in Figure 3.

Furthermore, it can be said that, in general, the large choice of currently available (and possible future) organic compounds that can be used as working fluids, and mixtures thereof, allow ORCs to be 'tuned' to specific applications. Therefore, ORCs comprise a more flexible solution by allowing some degree of control over the phase behaviour of the working fluid, the design of the processes that comprise the cycle, and in matching the cycle to available heat sources and heat sinks.

Performance Comparison with Rankine Cycles

In a previous section, when discussing Figure 2, a rudimentary analysis was used to indicate the underlying reasons for which ORCs may outperform conventional Rankine cycles when converting low-grade heat in small-scale systems. The current section proceeds to compare these two cycles directly, and to offer further insight into their relative performance, and also, the approximate cost of related power generation systems. Specifically, we focus here on a case study application where it is desired to generate electrical power from a fluid stream at an initial temperature of $T_{hot,in}$ = 200 °C. The heat source fluid stream is allowed to interact thermally with the heat engine, such that its enthalpy (and thus temperature) will decrease progressively as heat is taken in the cycle. This is similar to the rudimentary analysis that led to the result in Figure 2, only there the cycle was imagined to be an ideal, i.e. fully reversible, Carnot cycle, whereas here the cycle is a theoretical Rankine cycle with either water or an organic compound as the working fluid. The heat source fluid stream is taken to have a mass flow-rate $\dot{m}_{hot}$ = 500 kg/s and a specific heat capacity c_{phot} = 1 kJ/kgK, such that the stream duty is $(\dot{m}c_p)_{hot} = 5\times10^5$ W/K. Moreover, the heat sink (cooling) fluid stream has assumed to be an ambient temperature of 20 °C, and the condensation temperature and temperature at the inlet of pump, T_1, was taken to be 10 °C higher than this, T_1 = 30 °C.

Figures 6 and 7 show the specific work output and thermal efficiency, respectively, for a number of Rankine cycles operating with water and fluid R-245fa. Three lines are shown on each plot. Each one of these corresponds to a different saturation temperature (and thus also a different saturation pressure) during evaporation, as per the legend. Results for water-steam Rankine cycles are shown for the case of expansion to and condensation at: (i) 1 bar and 100 °C; and (ii) 0.04 bar and 30 °C. Clearly, it is thermodynamically beneficial, as stated previously, to expand to a low temperature that is as close as possible to atmospheric *temperature*, which in this case is 30 °C. However, this may come at a severe cost especially for small-scale systems, as discussed previously. Hence, expansion to near atmospheric *pressure* is also shown. Expansion to the lower temperature leads to a 2.5 – 4 fold increase in both specific work output and thermal efficiency.

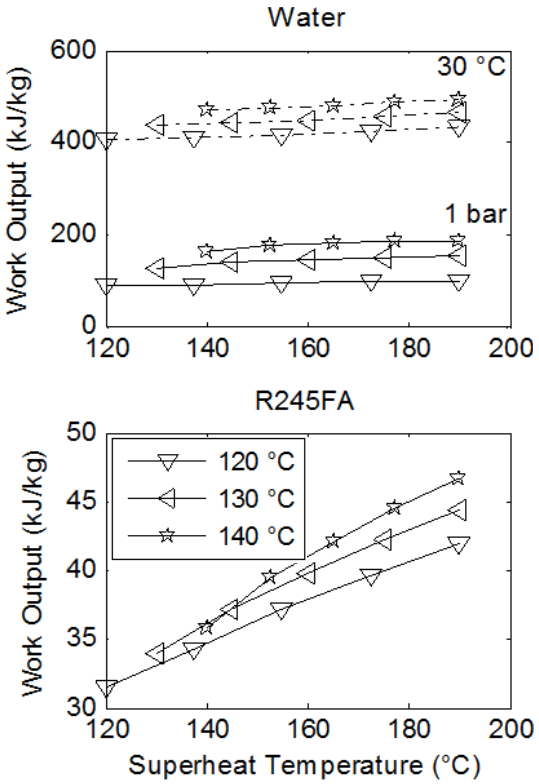

Figure 6 Comparison of specific work output, or power output per unit working fluid mass flow-rate, from Rankine cycles with water and R-245fa over a range of maximum cycle temperatures, T_3. The heat source fluid stream has an initial temperature $T_{hot,in}$ = 200 °C, a mass flow-rate $\dot{m}_{hot}$ = 500 kg/s and a specific heat capacity c_{phot} = 1 kJ/kgK. The 3 lines correspond to different evaporation (saturation) temperatures, given in the legend. Water results are shown for expansion down to (and condensation at) 1 bar/100 °C and 0.04 bar/30 °C.

In Figures 6 and 7, better performance (specific work *and* efficiency) can be observed at higher evaporation pressures. The extent of superheating does not strongly affect water-based cycle performance, but has a significant effect on work output from the ORCs, even though this does not appear in the ORC efficiencies. Essentially this is due to a near-proportional increase in both the heat input to the cycle along with the specific work output, as the degree of superheating is increased.

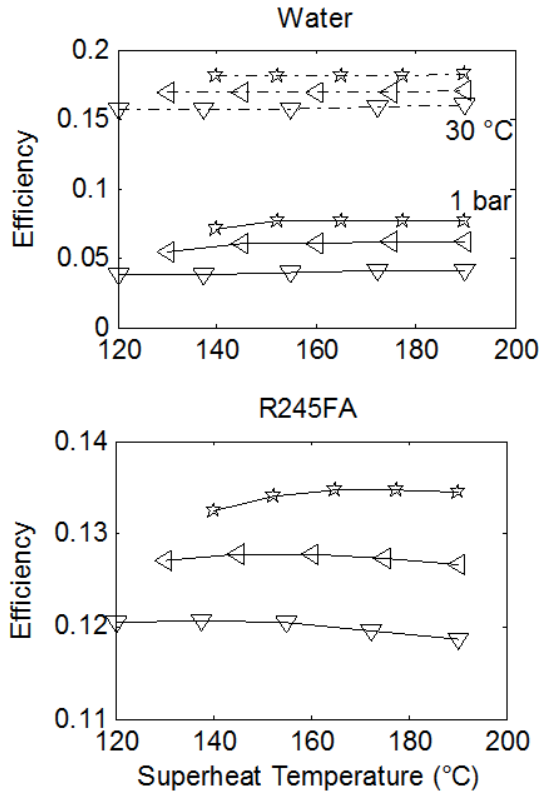

Figure 7 Comparison of cycle thermal efficiencies from Rankine cycles with water and R-245fa over a range of maximum cycle temperatures, T_3. Results correspond to the same conditions given in Figure 6.

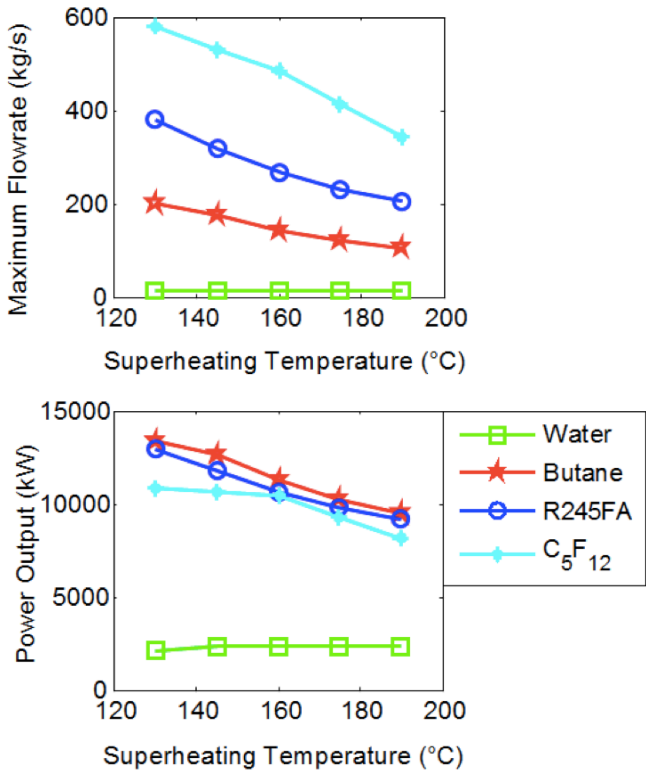

Figure 8 Maximum working fluid mass flow-rate and total power output from Rankine cycles with water and indicated organic fluids over a range of maximum cycle temperatures, T_3. Results correspond to the same conditions given in Figures 6 and 7. Water results are shown only for expansion down to (and condensation at) 1 bar/100 °C.

When comparing the two different working fluids, it is found that water outperforms the organic fluids with respect to specific work output by a factor of between 2 and 5 at the higher condensation pressure and temperature (for water). This increases to a factor of 10 or more at the lower condensation pressure and temperature. Although the specific work potential of the water cycles is always clearly higher than the equivalent potential of the organic fluid cycles, the performance in terms of efficiency presents a more mixed picture. In fact, at the higher condensation pressure and temperature for water, the organic fluids outperform water by a factor of 2 – 3, while at its lower condensation pressure and temperature water outperforms the organic fluids only marginally, by 3 – 4% absolute points, or 25 – 30% in relative terms.

Therefore, if one is to accept that it is not economically desirable to design a system in which steam is expanded down to and condenses at pressures of 0.04 bar, which is a reasonable point of view for affordable, distributed, small-scale power generation, ORCs show a potential for improved performance compared to conventional (water) Rankine cycles in terms of efficiency. Furthermore, it is important to consider not only the specific work output of these cycles, but the actual power output once the mass flow-rate of the working fluid is evaluated based on the thermal interaction between the heat engine cycle and the external heat source fluid stream. The result from such a consideration is shown in Figure 8, where we include data from three organic fluids: Butane, R-245fa and Perflenapent.

The results in Figure 8 were generated by progressively increasing the mass flow-rate of the working fluid in each cycle (i.e. each point on this plot) until a pinch temperature difference of 10 °C was reached in the evaporator between the heat source stream and the working fluid for that cycle. This is the maximum working fluid mass flow-rate. Interestingly, superheating is detrimental to ORC power output, but not to water. This figure demonstrates that, at least theoretically, organic fluids have the potential to outperform water by a considerable extent, also when considering power output in the chosen case study. In particular, power output for R-245fa is higher than that for water by a factor of 4 – 5. It is emphasised that this figure does not show water data at the low condensation conditions (0.04 bar and 30 °C). Nevertheless, the underlying conclusion remains unchanged, even when this data are considered. The organic fluids in this case outperform water by a factor between 1.5 and 2.

The observation that organic fluids have higher power outputs than water, even when compared to water condensing at the lower pressures and temperatures that showed higher specific work outputs (per unit mass flow-rate of working fluid) by more than an order of magnitude (recall Figure 6), can be understood by the much higher mass flow-rates permitted in ORCs before any pinch violation is reached. This can also be seen in Figure 8, and arises from the significantly higher specific enthalpy change during heat addition for water compared to the organic fluids, as indicated in Figure 4.

In Figure 9 a basic attempt is made at estimating approximate system costs. Here, we show the sum of costs associated with the purchase of the four basic components that form the Rankine heat engine systems. Each data point corresponds to the same systems contained in Figure 8. Heat exchanger costs were evaluated by using the C-value method, while costs for the pumps and expanders were obtained by compiling price information from a market study and establishing a correlation with component power, pressure ratio and flow-rate [17]. The C-value method is an approximate approach for the costing of heat exchangers, described in Hewitt *et al*. [18].

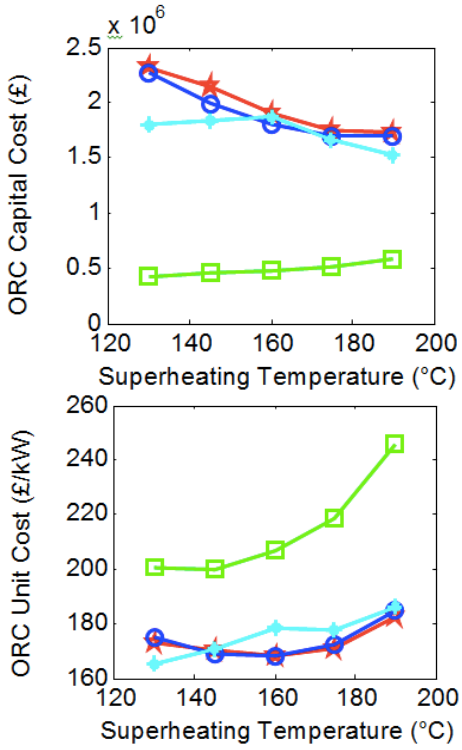

Figure 9 System costs corresponding to Figure 8, over a range of maximum cycle temperatures, T_3.

Figure 9 shows that, due to their larger heat exchangers (allowing higher power outputs) the ORCs are more expensive when considering the total system costs compared to water-based Rankine cycles. However, when the cost of the system is normalised by the power output capacity of the system, thus providing the all-important indicator of cost per unit useful output, the ORCs are shown to be a more affordable solution.

Finally, it is possible and instructive to condense the information contained in Figures 7 – 9 into a single performance-cost map. This is attempted in Figure 10. For simplicity and clarity, we do not show all data corresponding to each working fluid in this figure, which can be done by drawing an area for each working fluid. Instead, we select a single degree of superheating that corresponds to the maximum total power output. We recall, from Figure 8, that for organic fluids this is attained with little or no superheating. So, for example, for R-245fa this would be at an evaporation temperature of 120 °C, when the power output is ~ 14 MW and the cost per unit power ~ 195 £/kW.

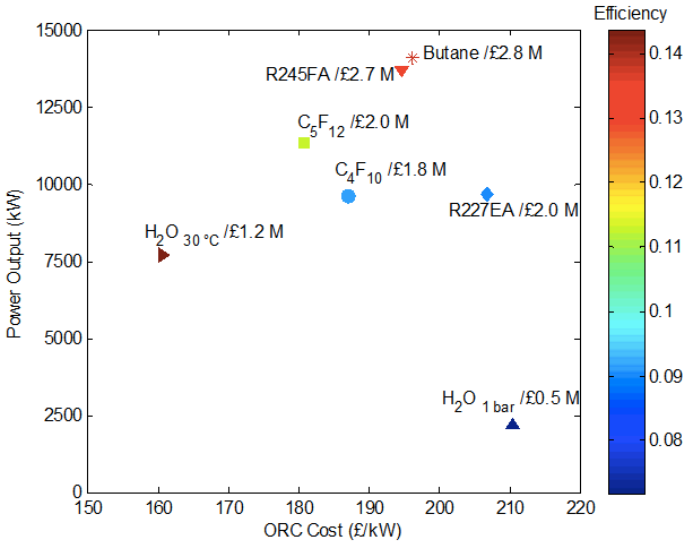

Figure 10 Consolidated plot of power output, efficiency and cost from Rankine cycles with water and indicated organic fluids corresponding to the results contained in Figures 7 – 9.

Opportunities for Improvement and Future Developments

It is well known from second law (exergy) analyses that about 75 – 80% of the ultimate potential to do useful work in a subcritical ORC is lost in the heat exchangers (evaporator, condenser, and regenerator) and about 20 – 25% in the expansion machine. The lost work (exergy destruction) in the evaporator amounts to approximately 1.5:1 – 2:1 times that lost in the condenser. Hence, further performance improvements can come from advances in these areas. Additionally, there is a great interest in the identification of optimal working fluids for specific applications. Recently, attention has turned to the utilisation of binary and even tertiary mixtures of organic compounds as working fluids in ORCs.

Advanced ORC system models that include a computer-aided molecular design (CAMD) framework with explicit information on the role of molecular size and structure on thermodynamic and thermal properties of working fluids are also currently in development [19], based on thermodynamic theories such as the statistical associated fluid theory (SAFT) [17,19]. Such models will play an important role in identifying optimal compromises between thermodynamic and thermal performance, which controls efficiency, power output, system size and cost. Furthermore, at the scales of operation of interest the selection of the expansion machine is an open question, with positive-displacement expanders presenting a real challenge to turbomachines. A significant effort is being made in the modelling and development of ORC systems featuring positive-displacement expanders, which promise higher efficiencies, for the applications identified in the present paper.

TWO-PHASE THERMOFLUIDIC OSCILLATORS

Definition

The term ‘thermofluidic oscillator’ was used in Ref. [20] to refer to an unsteady thermodynamic heat engine device within

which persistent and reliable thermodynamic property (pressure, temperature, etc.) oscillations are generated and sustained by constant temperature differences imposed by static (steady) external heat sources and sinks. The defining characteristic of such an unsteady heat engine is that the working fluid undergoes a thermodynamic cycle by virtue of the oscillatory time-varying flow of the working fluid through various connections (i.e. pipes, tubes) and into/out of any compartments within the device. In addition, these devices typically (but not necessarily) have no or few moving parts, reducing the need for dynamic seals. Oscillatory working fluid motion is then a necessary condition for the cycle to be observed during the operation of this device. This in direct contrast to conventional systems in which the cycle is undergone as the working fluid flows steadily from one individual component to the next, with each component responsible for a particular and well-defined process of the cycle. According to this definition thermofluidic oscillator devices include thermoacoustic engines [7,21-23], dry free-liquid-piston (Fluidyne) engines [24-27], free-piston Stirling engines [28-30], pulsejets and pulse-tubes [31-35].

Two-Phase Thermofluidic Oscillators (TFOs)

One type of thermofluidic oscillator that has been receiving attention is the 'two-phase thermofluidic oscillator' (TFO). The TFO shares the common feature of these types of thermodynamic systems in that reciprocating, positive-displacement work is produced by the sustained flow and pressure oscillations of the working fluid contained within the device. In particular, the TFO is a vapour-phase heat engine; the oscillatory operation and internal flows also establish a cyclic (periodic) two-phase thermal interaction with two heat exchangers (hot and cold) contained within the device. The hot heat exchanger introduces a high-temperature region inside the device that must be hotter than the saturation temperature of the working fluid at maximum pressure. Similarly, the cold heat exchanger introduces a cold-temperature region, which must be colder than the saturation temperature of the working fluid at minimum pressure. The alternating thermal interactions of the working fluid with the hot and cold regions result in a corresponding cyclic (periodic) evaporation and condensation of the working fluid. It is these alternating phase-change processes that induce the forcing necessary to sustain the thermodynamic cycle, and to drive the positive-displacement work done by the fluid in a suitable load.

Therefore, it can be noted that the key, defining characteristic of TFOs compared to thermoacoustic (TA) engines, Fluidyne and Stirling engine variants is their inherent reliance on phase change. Similarly to conventional steady heat engines, this choice carries a set of important advantages and also inevitable disadvantages. One key advantage arises from the high heat transfer coefficients that are associated with phase change, which can be an order of magnitude (or more) higher than those associated with single-phase forced convection. This allows significant heat transfer over relatively small temperature differences, which is important when dealing with low-grade heat sources, and also over smaller areas. In turn, it implies smaller, more compact and simpler heat exchangers, which has a direct implication on the eventual capital cost of these systems. It was previously stated that system cost for waste heat conversion technologies is an important consideration, and also that the electrical energy output per unit capital cost is an important consideration in this regard.

On the other hand, phase-change heat transfer can only be maintained at such high levels in a boiling regime close the critical heat flux (CHF), which occupies a narrow range of excess temperatures, i.e. the temperature differences between the walls of the heat exchangers and the working fluid, ΔT_e. To illustrate this point, Figure 11 that was generated based on a series of observations first by Nukiyama [36], the theoretical treatment of Kutateladze [37,38] and later by many investigators, indicates that the excess temperature should remain within the range 10 – 100 °C to maintain high levels of heat transfer coefficient not too far below the critical (maximum) heat flux nucleate boiling condition.

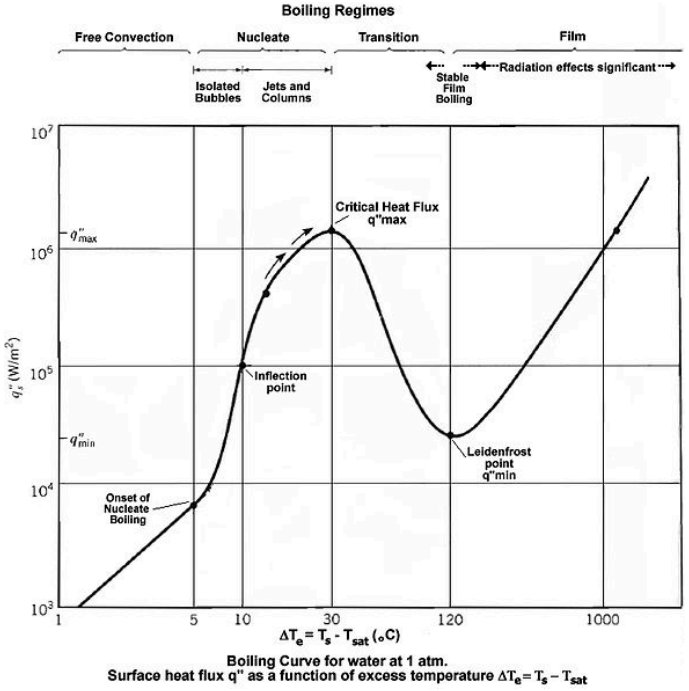

Figure 11 Heat flux for different boiling regimes as a function of excess temperature, $\Delta T_e = T_s - T_{sat}$, where T_s is the wall surface temperature at the fluid-solid interface and T_{sat} is the saturation temperature of the fluid. Taken from Ref. [39].

In addition, phase change imposes a limitation (saturation) on the temperature of the cycle during heat addition (evaporation) and heat rejection (condensation), which can give rise to exacerbated exergy (work) losses due to finite heat transfer across the increased temperature differences between the working fluid and the heat source and sink streams. This can be overcome by using fluid mixtures that exhibit a temperature 'glide' during phase change. This manifests in a gradually increasing phase-change temperature as evaporation proceeds (and *vice versa* for condensation), which can be used to thermally match the changing temperature of the heat source. However, this introduces an added level of complexity and our

fundamental understanding of these processes is still lacking. Various efforts are currently under way to improve our knowledge of the role of molecular size, structure and intermolecular forces and interactions in controlling these processes in both pure fluids, but also more importantly in this regard, for working fluid mixtures. This is a new and important development in this area, which promises noteworthy gains.

Non-Inertive-Feedback Thermofluidic Engine (NIFTE)

The Non-Inertive-Feedback Thermofluidic Engine (NIFTE) is a TFO concept that was first described in Refs. [20,40]. In this early work a small-scale laboratory prototype was constructed and a simple, spatially lumped linear dynamic model was developed in order to predict its oscillatory behaviour and performance. The early NIFTE prototype took the form of a pulsating, positive-displacement (liquid-piston) water pump with *n*-pentane as a working fluid [20]. The prototype was reported as being capable of operating across temperature differences as low as 30 K between the heat source and sink [41,42]. A simplified schematic of the NIFTE pump prototype as it appeared in Refs. [20,40] is given in Figure 12, along with a description of its main components in the caption.

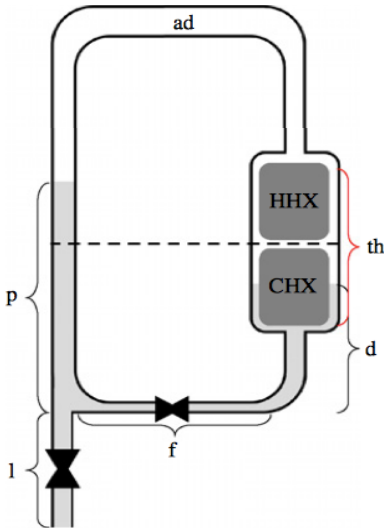

Figure 12 Schematic diagram of the early NIFTE device prototype. The hot heat exchanger (HHX) and cold heat exchanger (CHX) blocks are found within the combined thermal domain 'th'. The power and displacer (heat exchanger) cylinders are denoted by 'p' and 'd', the feedback connection and valve by 'f', and the load line by 'l' modelled by a valve. The connected vapour space above the liquid in the power and displacer cylinders, and also in the horizontal pipe connecting the two at their highest point, has been assumed previously (but not herein) to be an adiabatic vapour volume, denoted by 'ad'. The horizontal dashed line indicates the equilibrium (time-mean) liquid–vapour interface (liquid level) position in the two vertical cylinders. Taken from Ref. [43].

When operating with a 45 – 150 W heat source set at a temperature of 65 – 90 °C (via Joule heating in an electrical heating element embedded in the HHX), a heat sink at 4 – 12 °C (via the circulation of pumped cooling ice-water through the CHX) and with *n*-pentane chosen to be the working fluid with a 36 °C saturation temperature at the pumped pressure of around 1 atm., the NIFTE prototype demonstrated thermal efficiencies < 1% and exergy (second law) efficiencies up to 1.7% [20]. Since then, progress has been made on the development of a larger and updated solar-powered version of this technology using solar-thermal collectors to generate a hot stream of fluid, with recently reported thermal efficiency values up to about 1.5% and exergy efficiencies up to 9 – 10% at 80 °C heat source temperatures [42]. These values are expected to improve further, but to remain within the predicted range made in Ref. [1] for this technology, i.e. 1 – 5% and 5 – 20% respectively, depending on the characteristics of the device configuration, the application and the mode of operation.

The NIFTE efficiency values can be compared to: (i) the thermal efficiencies associated with Fluidyne engines, typically around 3 – 4%, and as high as 7% for some larger engines; (ii) the thermal efficiency from a standing-wave heat engine of 18.4%, reported by Backhaus and Swift [7] as recorded by Jin using the apparatus described by Godshalk *et al*. [44]; and (iii) the travelling-wave TA engine presented by Backhaus and Swift [7] whose thermal efficiency reached 24% when considering the power delivered to the load, and a maximum exergy efficiency of ~ 40% [45,46]. Nevertheless, as shown in Figure 1 in particular with respect to TA engines, it is noted that these engines are operated at significantly higher temperatures than the NIFTE (300 – 800 °C), with the higher efficiencies attained at the high end of this range, and hence the NIFTE retains its role at low temperatures (< 100 – 200 °C).

At this lower temperature end, well-designed Stirling engines may offer some competition (again, see Figure 1). It is the opinion of the author of the present paper that Stirling engines will emerge in the temperature range 80 – 200 °C with thermal efficiencies between 10 and 15 %, corresponding to exergy efficiencies in excess of 40 – 45%. Even so, these systems are complex in design and mechanical construction and operation, and are expected to be significantly more expensive to produce and to maintain. As mentioned previously, TFOs are capable of providing a more affordable alternative, albeit a less efficient one. The main competition for TFOs will arise from more inexpensive, simple ORC systems optimised to work at temperatures from 80 °C upwards. These should maintain a performance advantage compared to both Stirling and TFO systems such as the NIFTE. However, although ORC engines should be cost competitive compared to Stirling engines, they will inevitably be a higher cost solution than TFOs.

Although significant progress has been made on the NIFTE TFO over the past 12 years since the first laboratory prototype appeared, with efficiency performance improving by a factor of 5 or so over this timescale, there is scope for further improvement. This potential can be harnessed via an improved understanding of the fundamental underlying processes that govern the operation of this type of complex unsteady device, and the role of important components and variables in determining the device's operational characteristics and its performance. A concerted effort to develop a reliable model of the NIFTE is under way [41,43,47-51] by extending the spatially lumped and dynamic framework used in Refs. [20,40].

The aim of this on-going work is to produce a NIFTE device modelling tool for early-stage engineering design that requires little in terms of computational cost. This aspect is crucial as it allows the swift investigation of the design space, by allowing variations to a large number of design variables, ultimately leading to full multi-parametric system optimisation [52]. Still, the model must be capable of capturing underlying first-order effects and of predicting the trends of important operational parameters, such as frequencies of oscillation, and performance indicators, such as thermal and exergy efficiencies, flow rate and pressure oscillation amplitudes and phases.

Linearised Modelling Developments

A dynamic model of the NIFTE fluid pump was first presented in Refs. [20,40]. This model involved splitting the NIFTE device into well-defined sections, and developing spatially lumped, linearised first-order sub-models for each component section. Analogies were then drawn between the governing equations of each sub-model and linear passive electrical components, such as resistors (R), capacitors (C) and inductors (L) [43,53]. The component sub-models were interconnected to form an electrical circuit representation of the device, similar to the network shown in Figure 13. A similar approach had been used previously to model other *gas-phase* thermofluidic oscillators and was shown to be effective in capturing device behaviour to first-order [7,23,31].

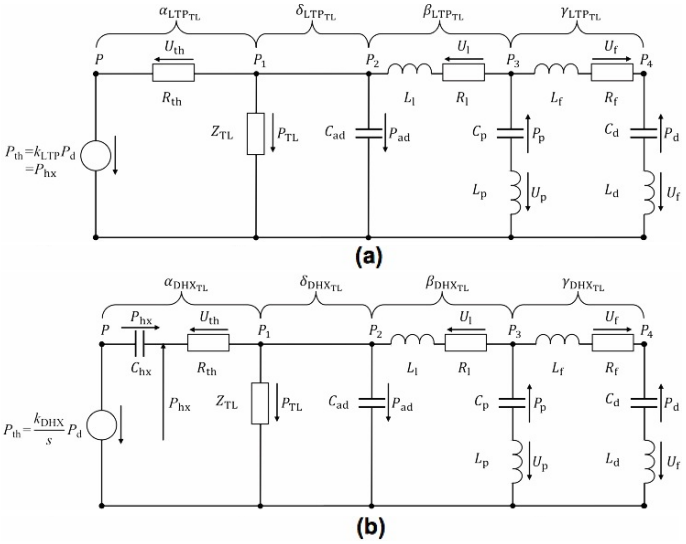

Figure 13 Electrical circuit representations of the NIFTE with a thermal (condensation) loss parameter (resistance R_{TL}) for the: (a) linear temperature profile (LTP); and (b) dynamic heat exchanger (DHX) models, where k_j corresponds to the feedback gain for model 'j', R_i to a resistance, C_i to a capacitance, L_i to an inductance, P_i to a pressure and U_i to a volumetric flow-rate. Subscript i = 'hx' refers to the heat exchangers, i = 'th' to the thermal domain, i = 'TL' to the unsteady thermal loss, i = 'ad' to the adiabatic vapour volume, i = 'l' to the load, i = 'p' to the power cylinder, i = 'd' to the displacer cylinder, and i = 'f' to the feedback line and valve. These networks were developed by using the methodology described in Refs. [20,30,41,43,47-51]. Taken from Ref. [43].

The first model of the NIFTE, presented in detail by Smith [20], added a description of the phase-change heat transfer processes that occur over the heat exchangers and a description of the exergetic losses due to irreversible heat transfer across the temperature differences between the working fluid and the heat exchangers. Further, this early model of the NIFTE assumed a static (steady) linear temperature profile (LTP) along the height of the heat exchangers in the thermal domain, and neglected all inertial effects of the working fluid in the liquid phase. In some regions of the parameter space, the model gave reasonable predictions of the oscillation frequency and exergetic efficiency observed in the NIFTE pulsating fluid-pump prototype, though in other cases the predictions deviated significantly from experimental results, both in magnitude and in capturing important trends of performance indicators such as operational frequency and efficiency when varying the main design parameters of the device [47].

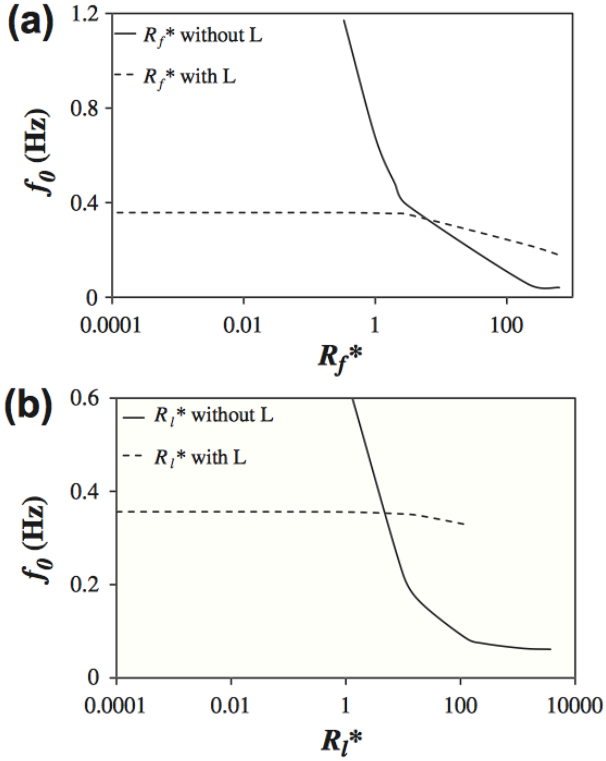

Figure 14 Predictions of the oscillation frequency of the NIFTE, f_0, from the non-inertive and inertive LTP models when varying the: (a) feedback resistance, R_f; and (b) load resistance, R_l. For the non-inertive case the plots are for f_0/10. Taken from Ref. [47].

In particular, the original model of the NIFTE assumed that flow inertia could be neglected when modelling this device. However, it is known that the working fluid in the liquid phase has a finite density, which should affect the dynamic behaviour of the device. Therefore, Markides and Smith [41] and also Solanki *et al.* [47] investigated the effect of introducing an explicit description of liquid flow inertia. This resulted in additional inductance terms that can be seen in Figure 13. The revised model was termed the 'inertive' LTP model. When comparing results from the inertive and original non-inertive

LTP models, it was found that the inclusion of inertia led to more realistic predictions of the critical temperature difference required in the heat exchangers for operation, and of the oscillation frequency of the NIFTE, f_0, as demonstrated in Figure 14. When interpreting Figure 14 one should bear in mind that experimental measurements demonstrated $f_0 = 0.1 – 0.2$ Hz for $R_f^* \approx 3 – 8$, $R_l^* \approx 80 – 290$ (as plotted in the figure) [20,43,47]. It was concluded that improved models of the NIFTE should include a description of the liquid flow inertia.

Another important aspect of the NIFTE concerns the two-phase heat transfer processes that take place between the hot and cold heat exchanger blocks and the working fluid inside the displacer cylinder (see Figure 12). Due to the high heat transfer coefficients the temperature on the surfaces of the HHX and CHX may respond dynamically to the thermal interaction with the working fluid. A revised model, termed 'dynamic heat exchanger' (DHX) model was developed specifically to account for this thermal interaction [43,49]. Results from this model showed an improved ability to capture the known behaviour of the existing NIFTE prototype device. An example of this improvement is demonstrated in Figure 15, which considers the operational frequency of the NIFTE device, f_0. Recall that experimental measurements demonstrated $f_0 = 0.1 – 0.2$ Hz for $R_f^* \approx 3 – 8$, $R_l^* \approx 80 – 290$ [20,43,47].

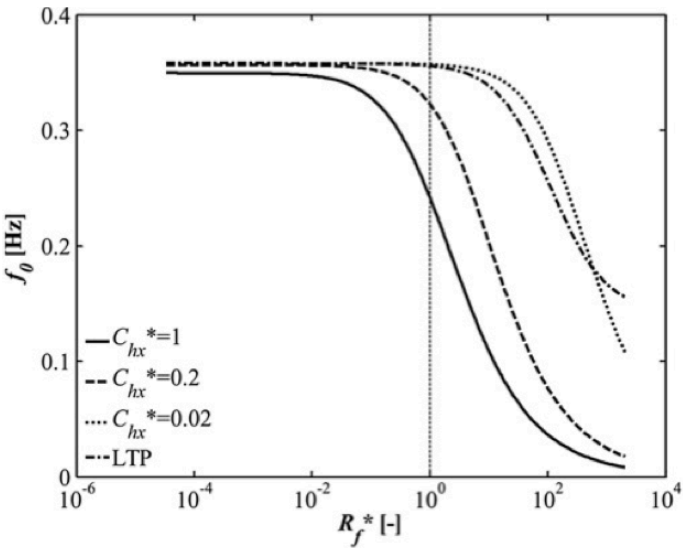

Figure 15 Predictions of the oscillation frequency of the NIFTE, f_0, from the inertive LTP and DHX models (at various heat exchanger thermal storage capacitances, C_{hx}*) when varying the feedback resistance, R_f. Taken from Ref. [49].

Nonlinear Modelling Developments

The inclusion of inertia and the revised modelling of the dynamic phase-change thermal processes between the heat exchangers and the working fluid in the displacer cylinder contributed to a reasonable prediction of the critical temperature difference required in the heat exchangers for operation of the NIFTE and its resulting oscillation frequency. Nevertheless, one feature of the NIFTE pumping device is that when a constant and low temperature difference is applied to the heat exchangers of the device, it exhibits sustained, robust periodic oscillations, with a specific characteristic amplitude and frequency that neither grow nor decay during steady-state operation. This behaviour persists despite known external thermal disturbances (i.e. variations) applied to the HHX and CHX blocks, and other inevitable natural disturbances to the operation of the device. This behaviour can be readily described as an 'asymptotically stable limit cycle', a characteristic associated exclusively with *nonlinear* dynamical systems. Therefore, although extremely useful in providing some local stability information and some insight into the actual operation and performance of the device, the linear models have noteworthy limitations with regards to their ability to predict reliably the behaviour of what is, actually, a nonlinear system. This motivated an effort to develop a nonlinear extension to the NIFTE model [48].

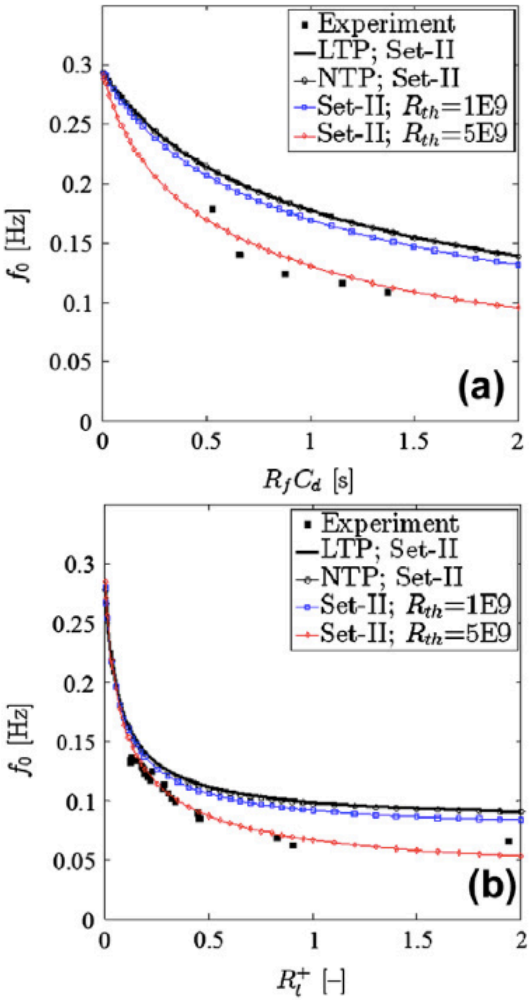

Figure 16 Predictions of the oscillation frequency of the NIFTE, f_0, from the linear NIFTE-LTP and nonlinear NIFTE-NTP models (at various heat exchanger thermal resistances, R_{th}) when varying the: (a) feedback resistance, R_f, and (b) load resistance, R_l. Comparison with experimentally obtained data points in Ref. [20]. All parameters are set to represent the NIFTE prototype in Ref. [20]. Taken from Ref. [48].

Figures 16 and 17 are from Ref. [48] and show a selection of predictions from the linear (NIFTE-LTP) and nonlinear (NIFTE-NTP) models, and comparisons with experimental data generated by performing tests on the NIFTE prototype pump reported in Ref. [20]. Figure 16 focuses on the operational frequency, f_0, and Figure 17a on the device exergy efficiency, η_{ex}. In both cases the models capture correctly the trends observed by the design corresponding to the NIFTE prototype that was used to generate the data on these plots.

Further parametric studies reported in Ref. [48] revealed that although both linear and nonlinear models of the NIFTE predicted similar oscillation frequencies, f_0, the nonlinear model predicted lower and more realistic exergy efficiencies, η_{ex}, over the envelope of investigated design parameters. This was attributed to the inability of the linear representation in the thermal domain to capture the saturation in the rate of heat exchange between the working fluid and the heat exchangers. In addition, Figure 17b indicates a reasonable prediction by the NIFTE-NTP of the experimentally obtained amplitudes of important thermodynamic properties around their equilibrium (time-mean) values, as well as of the phase angle between them. Shown in this Lissajous plot are the pressure in the vapour space, P_{ad}, and the volumetric variations in the load, V_l. Importantly, such a prediction of actual amplitudes of operation is one that that only a nonlinear model can make, with any linear description being inherently devoid of such a capability.

Thus, it can be concluded that the NIFTE-NTP model can capture the first order effects undergone by the NIFTE device within a range of operation that is close to that corresponding to the experimental prototype pump described in Refs. [20,40], and provide reasonable predictions of its dynamic behaviour and performance. However, even the NIFTE-NTP model requires an artificially increased value of the thermal resistance in the heat exchangers, R_{th} in order to match experimental data; considerably higher than the best estimate of this parameter for the NIFTE pump used to generate the data shown here. This is indicated in Figures 16 and 17 by showing results from using the best estimate value (designated 'Set-II') of $R_{th} = 0.8\times10^9$ kg/m^{4}s, and also results from artificially increased values of $R_{th} = 1\times10^9$ kg/m^{4}s and $R_{th} = 5\times10^9$ kg/m^{4}s. These changes in the value of R_{th} lead to relatively small deviations (< 0.05 Hz) in the predicted frequency of operation f_0 (Figure 16), but the predictions of the exergy efficiency η_{ex} are far more significantly affected. Specifically, the predicted efficiency values are overestimates of direct experimental observations by at factor of ~ 5 (Figure 17a). Improved predictions of the NIFTE's efficiency have been made, by including an additional loss component in the NIFTE model circuit [43]. This component accounts for the mechanism of *unsteady* parasitic condensation of the working fluid within the device away from the heat exchangers during operation. This is described in Figure 13 by the thermal loss resistance R_{TL}.

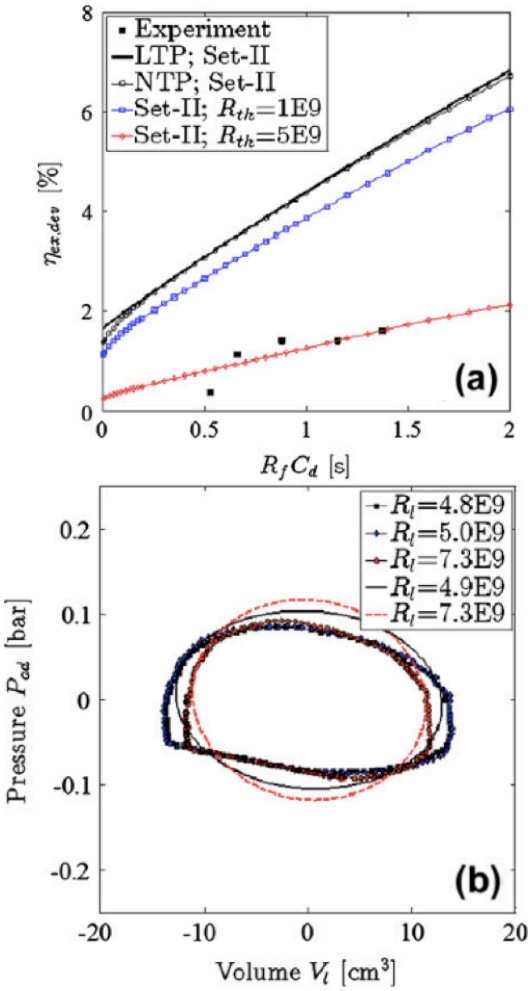

Figure 17 (a) Predictions of the device exergy efficiency, η_{ex}, from the linear NIFTE-LTP and nonlinear NIFTE-NTP models (at various heat exchanger thermal resistances, R_{th}). (b) Pressure–volume P_{ad}–V_l diagrams from the NTP model with a nonlinear gain corresponding to a HHX-CHX temperature difference of ΔT_{hx} = 60 K. Comparison with experimentally obtained data from Ref. [20]. All parameters are set to represent the NIFTE prototype in Ref. [20]. Taken from Ref. [48].

In summary, a series of simple dynamic system models with an increasing level of complexity are being devised to model the NIFTE. These models have allowed predictions of operational characteristics and performance indicators with progressively greater reliability and accuracy, leading to a better understanding of the capabilities of this technology as reported in Ref. [1]. The models are now also being translated to other similar dynamic systems with inherently unsteady operation. One example is the liquid Stirling engine (LSE) currently under development at the University of Twente in the Netherlands and the Boreskov Institute of Catalysis (BIC) in Novosibirsk, the Russian Federation [54].

FINITE HEAT TRANSFER EFFECTS

Thermally Induced Thermodynamic Losses

Time-mean heat transfer can act to affect heat engine performance detrimentally by giving rise a direct loss of the available heat from the heat source to the surroundings, which does not then take part in the thermodynamic cycle. This can be alleviated by careful design of the relevant components, for example by insulating the components and/or separating hot and cold sections in order to force thermal energy transport into the working fluid cycle. Beyond these losses, we have also come across two situations in which *unsteady* heat transfer (even in the case that the time-averaged heat transfer is zero) plays a significant role in affecting the performance of the energy conversion systems under consideration, as well as of similar systems. The first was in positive-displacement expansion machines that are being envisioned as high efficiency alternatives to turbomachines when used in small-scale ORC systems, and the second in the heat exchangers and in the nominally adiabatic vapour volumes of TFOs, such as the NIFTE.

Some peculiarities arise with respect to unsteady heat transfer in these systems owing to the fact that, unlike time-mean heat transfer, it is not possible to arbitrarily minimise this component of heat transfer with increasing levels of insulation. This is because a thin region of a solid (known as the thermal diffusion length, or 'penetration depth') that is in thermal contact with and experiencing time-varying heat exchange with a fluid domain, will also interact with the fluid in a time-varying manner and affect the magnitude and phase of the heat transfer process. This process and its detrimental effect on thermodynamic performance (also in the absence of time-mean heat transfer) is dealt with in the following sections.

Unsteady and Conjugate Heat Transfer

Unsteady and conjugate heat transfer is defined as a time-varying thermal energy transport process in which a solid is in thermal contact with a fluid, with both domains exhibiting a time varying temperature and heat flux at their common boundary, i.e. the solid-fluid interface. Figure 18 shows a conjugation map for a one-dimensional thermal interaction between a solid of finite thickness a and a fluid within which a flow imposes a constant convective heat transfer coefficient h. This map is plotted as a function of the Biot number, $Bi = ha/k_s$, where k_s is the thermal conductivity of the solid, and the Fourier number, $Fo = \alpha_s \tau / a^2$, where α_s is the thermal diffusivity of the solid and τ is the period of the temperature oscillations that are improved in the fluid domain due to some thermodynamic process.

The blue region in Figure 18 indicates large temperature fluctuations and small heat flux fluctuations (i.e. an isoflux boundary condition) on the solid-fluid interface, whereas the red region indicates large heat flux fluctuations and small temperature fluctuations on the same interface (i.e. an isothermal boundary condition). The large white square is an approximate narrow area occupied by the NIFTE prototype water pump as reported in Ref. [20], and the extended white space is the estimated design area within which the NIFTE technology can be expected to be found given reasonable present and future design variations from the initial design [41,43,47-52].

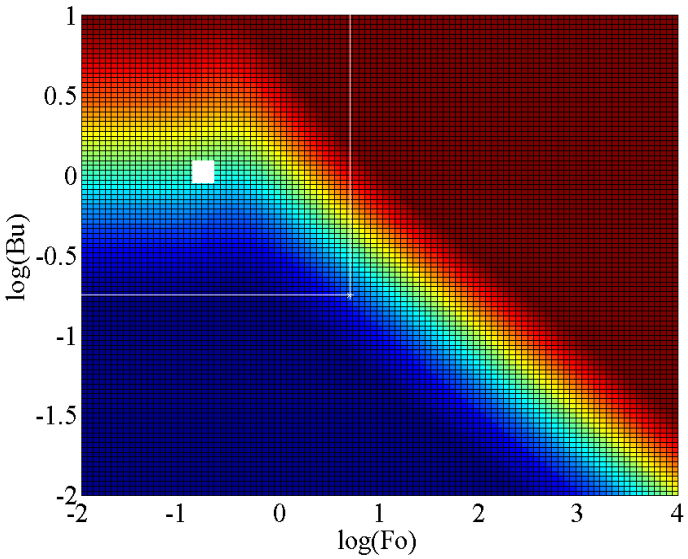

Figure 18 Map of conjugation, showing the extent of conjugation in unsteady 1-D solid-fluid systems, with an isoflux outer wall boundary condition. Blue indicates large temperature fluctuations and small heat flux fluctuations (approaching an isoflux boundary condition) on the wall surface at the solid-fluid interface and red indicates large heat flux fluctuations and small temperature fluctuations on the wall surface (approaching an isothermal boundary condition). The write space design area within which the NIFTE is expected.

It is evident that the region occupied by the NIFTE straddles the two extreme cases defined above. This implies that the boundary condition on the working fluid is neither isothermal nor isoflux, and that the solid and fluid are thermally coupled in such a way that in order to predict the temperature and heat flux at the solid-fluid interface the heat transfer problem must be solved in both domains and the solutions matched at this interface. This observation is important and has serious implications because it suggests that any effort to understand and predict the unsteady thermal losses in such a device must contain explicit information not just on the thermal processes in the fluid (i.e. heat transfer coefficients), but also in the solid which actively takes part in determining the thermal solution.

Case Study: Thermodynamic Losses in the NIFTE

Based on the observation made above, Solanki *et al*. [43] included a thermodynamic (exergy) loss mechanism into the modelling framework of the NIFTE that accounts for the unsteady conjugate heat transfer taking place in the vapour volume of the NIFTE, i.e. the top of the two vertical (power and displacer) cylinders in Figure 12. In a previous section, when presenting and discussing the findings from Ref. [43], it was stated briefly that predictions from the NIFTE-LTP and the NIFTE-DHX models were only able to capture the exergetic efficiencies, η_{ex}, observed experimentally by the device prototype when an additional dissipative thermal loss parameter that can account for this parasitic, cyclic phase-change thermal loss was included in both models. Figure 19 shows exergetic efficiency predictions from the LTP and DHX models with and without this thermal loss parameter.

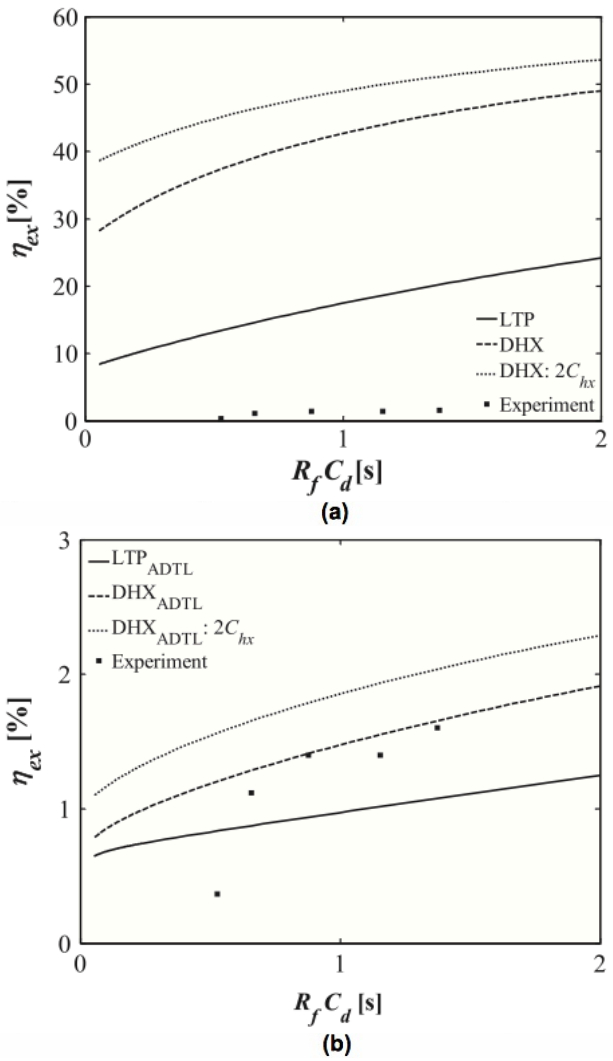

Figure 19 Exergy efficiency, η_{ex}, measurements and predictions from the inertive NIFTE-LTP and DHX models: (a) without a thermal loss parameter, and (b) with the thermal loss parameter and an adiabatic thermal condition imposed on the outside of the NIFTE device. Taken from Ref. [43].

The efficiency values in the absence of this mechanism are 11 and 30 times higher than those observed experimentally, for the LTP and DHX models respectively. The inclusion of the thermal loss parameter leads to a greatly improved prediction of the exergetic efficiencies of the prototype NIFTE pump by both the LTP and DHX models, both in trend and approximate magnitude. Thus, it can be concluded that, on accounting for this unsteady and conjugate thermal loss mechanism, the DHX model can provide adequate predictions of the key performance indicators of the NIFTE, that is, its oscillation frequency *and* the exergetic efficiency, suggesting that the important, first-order underlying processes taking place in the device are captured.

In addition to the efficiency, the inclusion of this loss mechanism allows a better prediction of the relative amplitudes and phases between important thermodynamic properties. Figure 20 shows pressure–volume P_{ad}–V_l Lissajous plots. As in Figure 19, both models show a vastly improved prediction capability, with the DHX model having a slight edge.

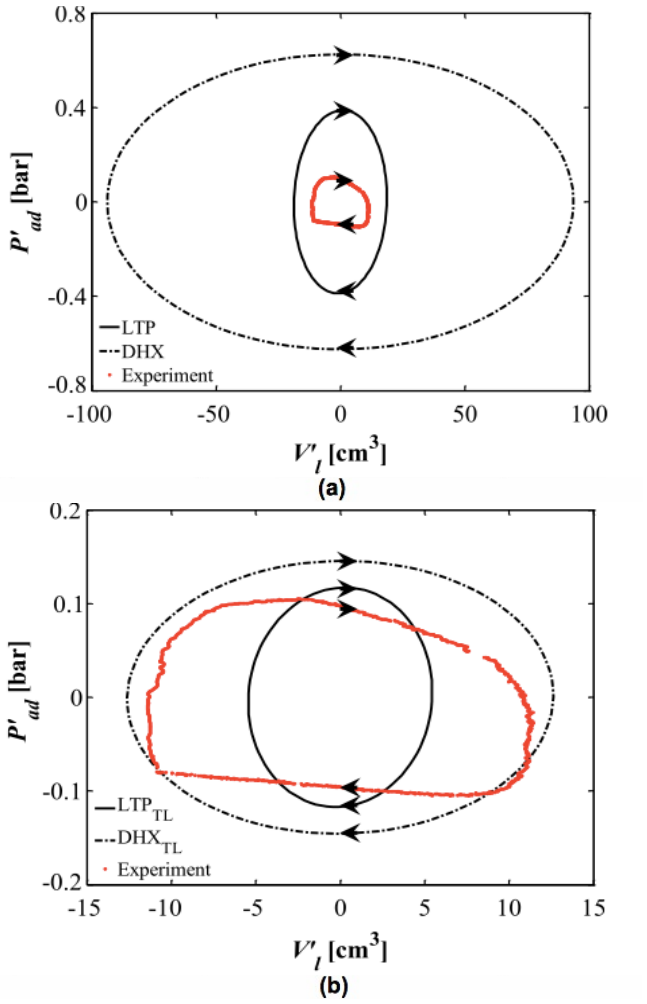

Figure 20 Time-resolved pressure–volume P_{ad}–V_l measurements and predictions from the inertive NIFTE-LTP and DHX models: (a) without a thermal loss parameter, and (b) with the thermal loss parameter. Taken from Ref. [43].

Thermodynamic Losses in Gas Springs

Mathie *et al*. [55] also considered the thermodynamic losses that result from cyclic, unsteady conjugate heat transfer in reciprocating components termed 'gas springs'. A gas spring is simplified model of a reciprocating compressor or expander, in which a fixed mass of gas is trapped in a cylinder, with a piston acting to impose volumetric variations. In the case considered in Ref. [55] the variations where sinusoidal, $V(t) = V_o + V_a \sin\omega t$, with a varying frequency, ω, whose dimensionless description is the Péclet number, $Pe = \omega D^2/\alpha_f$, where D is the diameter of the cylinder and α_f the thermal diffusivity of the fluid (gas). This arrangement is a convenient way to isolate the thermodynamic irreversibility due to thermal processes and remove those due to valve (pressure) losses. In addition to the frequency of the reciprocating motion, the framework allowed variations to the thickness and thermal properties of the solid walls of the cylinder, which are captured by the normalised cylinder wall thicknesses, a/δ, where $\delta = (2\alpha_s/\omega)^{0.5}$ is the thermal penetration depth. A result from the investigation in Ref. [55] is shown in Figure 21, which indicates the ability of the solid domain variables to affect the thermodynamic loss.

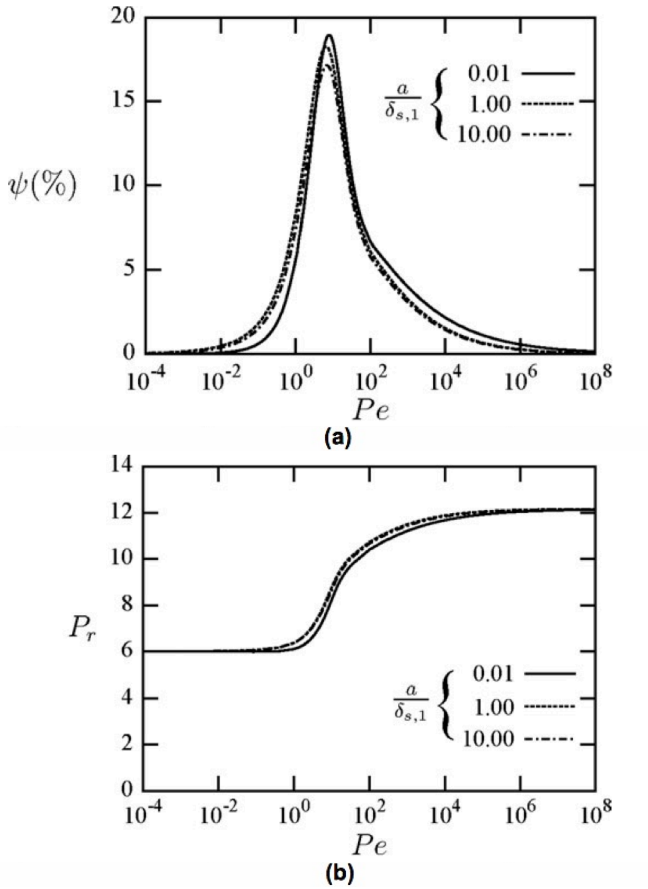

Figure 21 (a) Thermodynamic loss due to finite unsteady heat transfer, ψ, and (b) pressure ratio, in a reciprocating gas (air) spring with a volumetric compression ratio of 6 and for different normalised cylinder wall thicknesses, a/δ, as a function of Péclet number, Pe. Taken from Mathie *et al*. [55].

Nonlinear Heat Transfer Augmentation

We have so far considered the effects of unsteady and conjugate heat transfer for the case that the heat transfer coefficient, h, is set to a constant value, whether this is real or allowed to be a complex variable. The latter is the conventional approach taken when dealing with gas spring problems, in order to account for the observed phase shift between the heat flux at the wall and the temperature difference across the fluid [55-57]. One additional phenomenon is suspected to take place in the systems of interest, which is due to a nonlinear interaction between the (time-varying) heat transfer coefficient, h, and the (time-varying) temperature difference across the fluid domain, ΔT. This phenomenon is referred to as 'heat transfer augmentation' [56,57]. Mathematically, heat transfer augmentation can be described as follows; consider a fluid undergoing a time-varying thermal and fluid flow process, such that $\Delta T(t) = \overline{\Delta T} + \Delta T'(t)$ and $h(t) = \overline{h} + h'(t)$. Then, $\overline{q} = \overline{h\Delta T} = \overline{h}\,\overline{\Delta T} + \overline{h'\Delta T'} = A\overline{h}\,\overline{\Delta T}$. Essentially, this equation for the heat flux states that the fluctuations of the heat transfer coefficient, $h'(t)$, and those of the temperature difference, $\Delta T'(t)$, can become coupled. Physically, we would expect the instantaneous increase in the heat transfer coefficient to lead to a decrease in the instantaneous temperature difference, and *vice versa*.

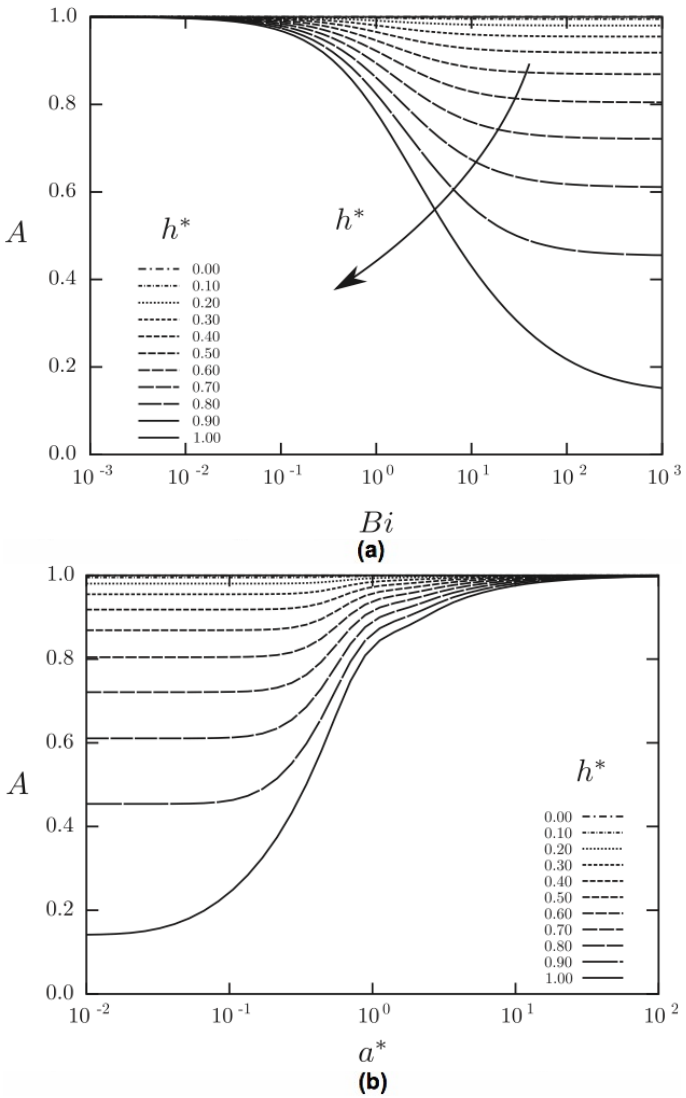

Figure 22 Augmentation ratio, $A = \overline{h\Delta T}/\overline{h}\,\overline{\Delta T}$, as a function of heat transfer coefficient fluctuation intensity ($h^* = h_a/h_o$; where the sinusoidally varying heat transfer coefficient is: $h(t) = h_o + h_a \sin\omega t$), Biot number ($Bi = h_o a/k$) and Fourier number ($a^* = a/\delta = \pi^{0.5}/Fo^{0.5}$). Taken from Mathie and Markides [56].

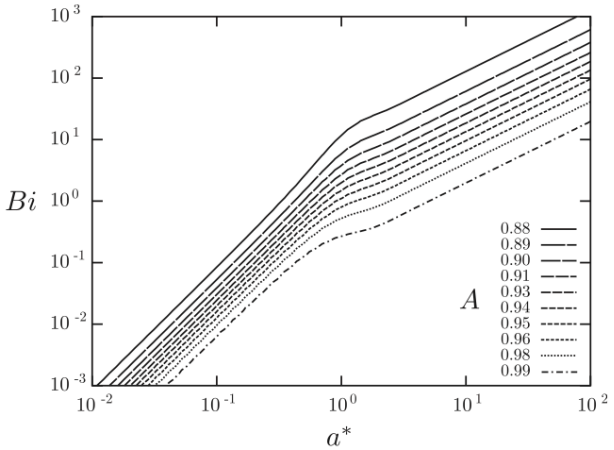

Figure 23 Combination of the augmentation plots in Figure 22 into a single map. Taken from Mathie and Markides [56].

Figures 22 and 23 show results from a semi-analytical study on the augmentation ratio, A, as a function of the: (i) heat transfer coefficient fluctuation intensity, $h^* = h_a/h_o$, where the sinusoidally varying heat transfer coefficient is: $h(t) = h_o + h_a \sin\omega t$, (ii) Biot number, $Bi = h_o a/k$, and (iii) the normalised solid wall thicknesses, $a^* = a/\delta$, where $\delta = (2\alpha_s/\omega)^{0.5}$ is the thermal penetration depth [56]. Note that in Figure 22a the normalised solid wall thickness is kept constant at $a^* = 1$, whereas in Figure 22b the Biot number is kept constant at $Bi = 1$. It can be observed that the augmentation ratio is always $A < 1$, suggesting a *reduction* in time-mean heat transfer relative to expectations from $\bar{q} = A\bar{h}\,\overline{\Delta T}$. Importantly, at small a^*, large h^* and/or large Bi this effect can become very significant.

The role of this phenomenon has not yet being considered in the energy conversion systems under consideration, but it has been identified and measured in a number of flows, such as in Refs. [56,57] which deal with two such cases: (i) the unsteady heat transfer between low-dimensional falling films and heated substrates, and (ii) the unsteady heat transfer between downstream of a broadband (turbulent) backwards-facing step. This forms an interesting and important avenue for further work.

CONCLUSION

This paper was concerned with energy technologies capable of converting heat at temperatures from 20 – 30 °C above ambient to 400 °C to useful power, aimed at the domestic (1 – 10 kWe) and commercial/industrial (10 – 100s of kW) sectors, thus covering a range of power output scales from a 1 kW to 1 MW. Two distinct classes of systems were considered, both based on thermodynamic vapour-phase heat engine cycles undergone by organic working fluids, namely organic Rankine cycles (ORCs) and two-phase thermofluidic oscillators (TFOs).

ORCs are a more well-established and mature technology, are more efficient, especially with higher temperature heat sources and at larger scales, whereas TFOs are more cost-competitive, in particular at lower temperatures and smaller scales. Specifically, ORC systems are particularly well-suited to the conversion of low- to medium-grade heat (i.e. heat source temperatures up to about 300 – 400 °C) to mechanical or electrical work, and at an output power scale from kW up to a few 10s of MW. Thermal efficiencies in excess of 25% are achievable at the higher temperatures, and efforts are currently in progress to develop improved systems by focussing on working fluid selection, the heat exchangers and expansion machines at the scale of interest. Correspondingly, TFO systems are a more recent development aimed at the affordable conversion of low-grade heat (i.e. hot temperatures from 20 – 30 °C above ambient, up to approximately 100 – 200 °C) to hydraulic work for fluid pumping and/or pressurisation with a thermal efficiency (ultimately) of 1 – 5%.

In both cases, models capable of accurate and reliable predictions of system performance were used to provide insight on operational characteristics and performance. Challenges and opportunities were identified, and recommendations made for further improvements, in particular with regards to the minimisation of thermodynamic losses inflicted by finite heat transfer effects. It was shown that these losses can arise from inherently unsteady, conjugate and nonlinear thermal processes between the working fluids within the systems of interest and the solid walls of key system components.

REFERENCES

[1] Markides C.N., The role of pumped and waste heat technologies in a high-efficiency sustainable energy future for the UK, *Applied Thermal Engineering,* Vol. 53, 2013, pp. 197-209

[2] Lawrence Livermore National Laboratory, Estimated U.S. energy in 2013, *from* https://flowcharts.llnl.gov [accessed 20 April 2014], 2014.

[3] European Commission, EU-27 streamlined energy flow trends – 2006; Supply transformation, consumption (PJ), *from* https://groups.google.com/forum/#!topic/energy-discussion-group/Jy9rvgY-P04 [accessed 20 April 2014], 2011.

[4] Smith C.A., Belles R.D., and Simon A.J., Estimated international energy flows; 2007, *Report*, Lawrence Livermore National Laboratory, Livermore (CA), 2011.

[5] Bianchi M., and Pascale A.D., Bottoming cycles for electric energy generation: Parametric investigation of available and innovative solutions for the exploitation of low and medium temperature heat sources, *Applied Energy*, Vol. 88, 2011, pp. 1500-1509

[6] Nightingale N.P., Automotive Stirling engine; Mod II design report, *Report DOE/NASA/0032-28; NASA CR-175106; MT186ASE58SRI*, National Aeronautics and Space Administration, Cleveland (OH), 1986.

[7] Backhaus S., and Swift G.W., A thermoacoustic-Stirling heat engine: Detailed study, *Journal of the Acoustical Society of America*, Vol. 107, 2000, pp. 3148-3166

[8] Snyder G.J., and Toberer E.S., Complex thermoelectric materials, *Nature Materials*, Vol. 7, 2008, pp. 105-114

[9] Jing-Feng Li, Wei-Shu Liu, Li-Dong Zhao, and Min Zhou, High-performance nanostructured thermoelectric materials, *NPG Asia Materials*, Vol. 2, 2010 pp. 152-158.

[10] Szczech J.R., Higgins J.M., and Jin S., Enhancement of the thermoelectric properties in nanoscale and nanostructured materials, Journal of Materials Chemistry, Vol. 21, 2011, pp. 4037-4055

[11] Hsu K.F., Loo S., Guo F., Chen W., Dyck J.S., Uher C., Hogan T., Polychroniadis E.K., and Kanatzidis M.G., Cubic $AgPb_mSbTe_{2+m}$: Bulk thermoelectric materials with high figure of merit, *Science*, Vol. 303, 2004, pp. 818-821

[12] Biswas K., He J., Blum I.D., Wu C.-I., Hogan T.P., Seidman D.N., Dravid V.P., and Kanatzidis M.G., High-performance bulk thermoelectrics with all-scale hierarchical architectures, *Nature*, Vol. 489, pp. 414-418

[13] Vining C.B., An inconvenient truth about thermoelectrics, *Nature Materials*, Vol. 8, 2009, pp. 83-85

[14] Royal Academy of Engineering, The costs of generating electricity; A study carried out by PB power for the Royal Academy of Engineering, *from* http://www.raeng.org.uk/news/publications/list/reports/Cost_of_Generating_Electricity.pdf [accessed 20 April 2014], 2004.

[15] Gullì F., Small distributed generation versus centralised supply: A social cost–benefit analysis in the residential and service sectors, *Energy Policy*, Vol. 34, 2006, pp. 804-832

[16] Strachan N., and Farrell A., Emissions from distributed vs. centralized generation: The importance of system performance, *Energy Policy*, Vol. 34, 2006, pp. 2677-2689

[17] Oyewunmi, O.A., Taleb, A.I., Haslam A.J., and Markides C.N., An assessment of working-fluid mixtures using SAFT-VR Mie for use in organic Rankine cycle systems for waste-heat recovery, *Computational Thermal Sciences*, accepted, to appear, 2014

[18] Hewitt G.F., Shires G.L., and Bott T.R., Process Heat Transfer, CRC Press, London, 1994.

[19] Lampe, M., Gross, J., and Bardow, A., Simultaneous process and working fluid optimisation for organic Rankine cycles (ORC) using PC-SAFT, *Computer-Aided Chemical Engineering*, Vol. 30, 2012, pp. 572-576
[20] Smith T.C.B., Thermally driven oscillations in dynamic applications, *PhD Thesis*, University of Cambridge, Cambridge, 2006.
[21] Wheatley J., Hofler T., Swift G.W., and Migliori A., An intrinsically irreversible thermoacoustic heat engine, *Journal of the Acoustical Society of America*, Vol. 74, 1983, pp. 153-170
[22] Wheatley J., Hofler T., Swift G.W., and Migliori A., Experiments with an intrinsically irreversible acoustic heat engine, *Physical Review Letters*, Vol. 50, 1983, pp. 499-502
[23] Ceperley P.H., A pistonless Stirling engine–The travelling wave heat engine, *Journal of the Acoustical Society of America*, Vol. 66, 1979, pp. 1508-1513
[24] West C., The Fluidyne heat engine, *Research report*, Report No. AERE-R 6775, Harwell, Atomic Energy Research Establishment, 1971.
[25] West C.D., and Pandey R.B., Laboratory prototype Fluidyne water pump, IECEC 1981: Proceedings of the 16th Intersociety Energy Conversion Engineering Conference, Atlanta (GA), 9-14 August 1981, pp. 1916-1918.
[26] West C.D., Dynamic analysis of the Fluidyne, IECEC 1983: Proceedings of the 18th Intersociety Energy Conversion Engineering Conference, Orlando (FL), 21-26 August 1983, pp. 779-784.
[27] Stammers C.W., The operation of the Fluidyne heat engine at low differential temperatures, *Journal of Sound and Vibration*, Vol. 63, 1979, pp. 507-516
[28] Redlich R.W., and Berchowitz D.M., Linear dynamics of free-piston Stirling engines, *Proceedings of the Institution of Mechanical Engineers, Part A: Power and process engineering*, Vol. 199, 1985, pp. 203-213
[29] Walker G., and Senft J.R., Free piston Stirling engines, Springer, Berlin, 1985.
[30] Wood J.G., and Lane N.W., Advanced 35 We Stirling engine for space power applications, El-Genk M.S. (Ed.), STAIF 2003: Proceedings of the Space Technology and Applications International Forum, Albuquerque (NM), 2-5 February 2003, pp. 662-667.
[31] Huang B.J., and Chuang M.D., System design of orifice pulse-tube refrigerator using linear flow network analysis, *Cryogenics*, Vol. 36, 1996, pp. 889-902
[32] Payne P.R., Brown R.G., and Brown J.P., Water pulsejet research, Final report Payne Inc., Annapolis (MD) (April 1979) Report No. DOE/ET/20288–T1.
[33] Kentfield J.A.C., Fundamentals of idealized airbreathing pulse-detonation engines, *Journal of Propulsion and Power*, Vol. 18, 2002, pp. 78-83
[34] Kentfield J.A.C., Thermodynamics of airbreathing pulse-detonation engines, *Journal of Propulsion and Power*, Vol. 18, 2002, pp. 1170-1175
[35] Organ A.J., Stirling and pulse-tube cryo-coolers, 1st ed., John Wiley and Sons, Bury St. Edmunds, 2005.
[36] Nukiyama S., Film boiling water on thin wires, *Society of Mechanical Engineering*, Japan, Vol. 37, 1934.
[37] Kutateladze S.S., Hydromechanical model of the crisis of boiling under conditions of free convection, *Journal of Technical Physics*, USSR, Vol. 20, 1950, pp. 1389-1392
[38] Kutateladze S.S., Boiling heat transfer, *International Journal of Heat and Mass Transfer*, Vol. 4, 1961, pp. 31-45
[39] deGrazia, J., *from* http://youtu.be/429BC2KZV7A [accessed 20 April 2014], 2014.
[40] Smith T.C.B, Power dense thermofluidic oscillators for high load applications, IECEC 2004: Proceedings of the 2nd International Energy Conversion Engineering Conference, Providence (RI), 16-19 August 2004, pp. AIAA-2004-5758/1-15.
[41] Markides C.N., and Smith T.C.B., A dynamic model for the efficiency optimization of an oscillatory low grade heat engine, *Energy*, Vol. 36, 2011, pp. 6967-6980
[42] Thermofluidics, *from* http://www.thermofluidics.co.uk [accessed 20 April 2014], 2014.
[43] Solanki R., Mathie R., Galindo A., and Markides C.N., Modelling of a two-phase thermofluidic oscillator for low-grade heat utilisation: Accounting for irreversible thermal losses, *Applied Energy*, Vol. 106, 2013, pp. 337-354
[44] Godshalk, K.M., Jin C., Kwong Y.K., Swift G.W., and Radebaugh R., Characterization of 350 Hz thermoacoustic driven orifice pulse tube refrigerator with measurements of the phase of the mass flow and pressure, *Advanced Cryogenic Engineering*, Vol. 41, 1996, pp. 1411-1418
[45] Backhaus S., and Swift G.W., A thermoacoustic-Stirling heat engine, *Nature*, Vol. 399, 1999, pp. 335-338
[46] Backhaus S., and Swift G.W., Fabrication and use of parallel-plate regenerators in thermoacoustic engines, IECEC 2001: Proceedings of the 36th Intersociety Energy Conversion Engineering Conference, Savannah (GA), 29 July-2 August 2001, pp. 453-458
[47] Solanki R., Galindo A., and Markides C.N., Dynamic modelling of a two-phase thermofluidic oscillator for efficient low grade heat utilization: Effect of fluid inertia, *Applied Energy*, Vol. 89, 2012, pp. 156-163
[48] Markides C.N., Osuolale A., Solanki R., and Stan G.-B.V., Nonlinear heat transfer processes in a two-phase thermofluidic oscillator, *Applied Energy*, Vol. 104, 2013, pp. 958-977
[49] Solanki R., Galindo A., and Markides C.N., The role of heat exchange on the behaviour of an oscillatory two-phase low-grade heat engine, *Applied Thermal Engineering*, Vol. 53, 2013, pp. 177-187
[50] Markides C.N., and Gupta A., Experimental investigation of a thermally powered central heating circulator: Pumping characteristics, *Applied Energy*, Vol. 110, 2013, pp. 132-146
[51] Markides C.N., Solanki R., and Galindo A., Working fluid selection for a two-phase thermofluidic oscillator: Effect of thermodynamic properties, *Applied Energy*, Vol. 124, 2014, pp. 167-185
[52] Palanisamy K., Taleb A., and Markides C.N., Optimising the non-inertive-feedback thermofluidic engine for the conversion of low-grade heat to pumping work, *Heat Transfer Engineering*, accepted, to appear, 2014
[53] Care C., Technology for modelling: Electrical analogies, engineering practice and development of analogue computing, Springer Verlag, New York (NY), 2010.
[54] Glushenkov M., Sprenkeler M., Kronberg A., and Kirillov V., Single-piston alternative to Stirling engines, *Applied Energy*, Vol. 97, 2012, pp. 743-748
[55] Mathie R., Markides C.N., and White A.J., A Framework for the Analysis of Thermal Losses in Reciprocating Compressors and Expanders, *Heat Transfer Engineering*, accepted, in press, 2014
[56] Mathie R., and Markides C.N., Heat transfer augmentation in unsteady conjugate thermal systems – Part I: Semi-analytical 1-D framework, *International Journal of Heat and Mass Transfer*, Vol. 56, 2013, pp. 802-818
[57] Mathie, R., Nakamura, H., and Markides, C.N., Heat transfer augmentation in unsteady conjugate thermal systems – Part II: Applications, *International Journal of Heat and Mass Transfer*, Vol. 56, 2013, pp. 819-833